

When Robotics Meets Wireless Communications: An Introductory Tutorial

Daniel Bonilla Licea⁺ *Member, IEEE*, Mounir Ghogho^{†*}, *Fellow Member, IEEE*, and Martin Saska⁺,

⁺Czech Technical University in Prague, Czech Republic

[†]International University of Rabat, College of Engineering & Architecture, TICLab, Morocco

^{*} School of Electronic and Electrical Engineering, University of Leeds, UK

bonildan@fel.cvut.cz, m.ghogho@ieee.org, martin.saska@fel.cvut.cz

Abstract—The importance of ground Mobile Robots (MRs) and Unmanned Aerial Vehicles (UAVs) within the research community, industry, and society is growing fast. Many of these agents are nowadays equipped with communication systems that are, in some cases, essential to successfully achieve certain tasks. In this context, we have begun to witness the development of a new interdisciplinary research field at the intersection of robotics and communications. This research field has been boosted by the intention of integrating UAVs within the 5G and 6G communication networks. This research will undoubtedly lead to many important applications in the near future. Nevertheless, one of the main obstacles to the development of this research area is that most researchers address these problems by oversimplifying either the robotics or the communications aspect. This impedes the ability of reaching the full potential of this new interdisciplinary research area. In this tutorial, we present some of the modelling tools necessary to address problems involving both robotics and communication from an interdisciplinary perspective. As an illustrative example of such problems, we focus in this tutorial on the issue of communication-aware trajectory planning.

Index Terms—Communication, control, trajectory planning, robot, UAV.

I. INTRODUCTION

Interdisciplinary research involving communications and robotics is gaining momentum, as evidenced by the steady increase in publications by the robotics [1], [2], [3], [4], control [5], [6], [7], [8], [9] and the communications [10], [11], [12], [13], [14], [15], [16], [17] communities dealing with Mobile Robots (MRs) and communications issues. Some reasons behind this growing interest include the emergence of a 5G technology that aims to integrate Unmanned Aerial Vehicles (UAVs) in the cellular communication network [18], [19] and the growing importance of robotic swarms [20]. From an application perspective, we can divide these interdisciplinary problems into two categories: Robotics-assisted Communications (RaC) and Communications-assisted Robotics (CaR).

In RaC applications, generally one or multiple MRs are incorporated into a communication network with the intent to improve the performance of the latter; the MRs typically operate as mobile relays, data ferries, or mobile flying Base Stations (BSs) on-board Unmanned Aerial Vehicles (UAVs). The main objective of RaC is to control the behavior of

This work was partially funded by the European Union's Horizon 2020 research and innovation programme AERIAL-CORE under grant agreement no. 871479.

the added MR in order to improve the performance of the communications network. In traditional mobile communications, the transceiver's position is considered *uncontrollable* and random. In RaC, the transceiver's position is *controllable*, and thus constitutes an additional communication system parameter to be optimized. This small but important difference opens up new and exciting possibilities in the design of communication systems involving MRs. For example, in the context of diversity techniques for the small-scale fading compensation, it is widely accepted that designing the diversity branches in such a way as to make the channels statistically independent maximizes the diversity gain and thus performance. By analyzing the same problem while considering a transceiver mounted on a MR, we demonstrated in [21] that by controlling and adapting the MR's position, we can obtain diversity branches that yield a higher diversity gain than that obtained with statistically independent branches. This short example provides a brief glimpse into the possibilities of going beyond old theoretical bounds stated in classical communication problems by considering the controlled mobility of the transceiver as an additional degree of freedom.

In CaR applications, the communication capabilities of the MR are leveraged to help the robotic system to better perform some tasks. Communication is an essential component that enables multi-robot applications [22] and UAV swarms [20], [23], [3]. Communication between the MRs allow to exchange different types of information, such as: relative localization that allows for the creation of formations or the navigation of surroundings in a coordinated manner; sensing data that could be used in mapping applications; signalisation data to coordinate the behaviour of the team, etc. Often in CaR applications, the MRs must execute certain robotic tasks while considering the communication quality and swarm connectivity to ensure adequate behaviour of the robotic team.

To efficiently address the problems encountered in RaC and CaR applications, we argue that a good understanding of *both* communications and robotics is required. Indeed, as will be described later, there is often a deep entanglement between the communications and robotics aspects in such problems. Considering only the communications aspects and oversimplifying the MR's model might produce an energy inefficient solution that wastes too much energy in motion, or even an unfeasible solution for a real MR due to a breach of its own mechanical constraints. On the other hand, focusing on

the robotics aspects and oversimplifying the communication model may lead the MR to fail to complete its task due to unexpected communication failures, which may arise from poorer connectivity or a lower bit rate than that expected with the oversimplified model. Therefore, an interdisciplinary approach is essential when dealing with CaR and RaC problems in order to propose functionally adequate solutions and to fully exploit all underlying opportunities in this new research area. The importance of such interdisciplinary approach has also been recently recognized in [24], [25] where the authors propose a simulation framework that allows to coordinate a robotics simulator (ROS), a communications network simulator, and an antenna simulator. This enables to accurately simulate the dynamics of the robot and the communications channel.

In the literature, however, CaR and RaC problems are often not addressed with such an interdisciplinary approach. Indeed, oversimplified models are often adopted for either the communications or the robotics aspects. This oversimplification causes the researchers to miss interesting results and opportunities. Even worse, the researchers could derive techniques that will fail when tested on real robots equipped with real communication systems. Some tutorials have recently been published on communications-aware robotics problems, but these simplify either the robotics or communications aspects. For instance, the tutorial [19] discusses UAV communications with great detail from the communications perspective, but treats the control and robotics aspects in a superficial manner. The authors in [19] mention that, to the best of their knowledge, no rigorous expression for the UAV energy consumption for a given trajectory has been derived. As we will show in Subsection II-B, such a statement is imprecise and comes from a lack of understanding of the UAV dynamic models and control theory. On the other hand, the robotics community generally oversimplifies the communication model. For instance, the authors of [26] consider the problem of a team of data-gathering MRs, and assume a binary disk model [27] for the communication channel; in this model, the communication is perfect as long as two MRs remain within a certain distance of each other. This communication model is far from reality, as we shall see in section III-A.

To our knowledge, in the literature, there are no surveys or tutorials which have taken an interdisciplinary approach to address CaR or RaC problems. The aim of this tutorial is to contribute to filling this gap and raising awareness of the importance of an interdisciplinary approach when tackling these problems. To illustrate the opportunities and challenges of this approach, we focus on the important problem of Trajectory Planning (TP) within the context of CaR and RaC applications, henceforth referred to as Communications-aware Trajectory Planning (CaTP). We hope that this tutorial will contribute to the quality and quantity of research done in this new exciting and promising, yet underdeveloped, research area.

This tutorial is organized as follows. In section II, we describe in detail the basic and crucial mobile robotics aspects and models. Section III describes different aspects of communications systems which are relevant to CaTP problems and

discusses modelling of the wireless communication channels. In section IV, the general structure of various CaTP problems, different types of cost functions, and constraints involved in these problems are described. Finally, section V provides conclusions and discusses some open research problems and opportunities.

II. MOBILE ROBOT MODELING

We can classify the Mobile Robots (MRs) according to their operational environment (e.g. aerial robots, ground robots, underwater robots, unmanned surface vehicles, amphibian robots), and also according to their locomotion mechanism (e.g. wheels, legs). The objective of this section is to provide the reader with the basic knowledge and mathematical models of MRs deemed necessary to address problems that are at the intersection of robotics and communications. We do not intend to provide an extensive exposition of the subject; we will discuss only three of the most popular types of MRs: ground wheeled robots, multirotor aerial robots, and fixed-wing aerial robots. These types of MRs have been used in various CaTP applications and in common industrial deployments of MR. Before we discuss these MRs, let us briefly discuss the modelling process and its importance in the context of trajectory planning problems.

Mathematically modelling a phenomenon or object consists of describing it in terms of certain aspects of interest and under certain conditions by means of analytical mathematical equations and/or numerical models. We can divide the mathematical model into four components:

- 1) **Object representation:** in our case, the object to be modelled is the MR. The object representation is a mathematical abstraction of the physical MR that describes properties that are relevant for the problem at hand. In the context of trajectory planning problems, the MR can be described as a single point¹ with orientation, even if the real object itself occupies non-zero physical space. This is a suitable representation of the MR for trajectory planning problems, but it may be inadequate for other problems, such as the mechanical analysis of the MR's frame.
- 2) **Model Input:** the model input is a set containing all controllable variables and whose effect on the object representation will be captured by the mathematical model. There might be other controllable variables which affect the object representation, but the model input includes only the variables considered in the mathematical model.
- 3) **Range of validity:** this consists of all the conditions under which the model will adequately describe the behaviour of the object representation, e.g. the assumptions on the considered scenarios, ranges of variations for the variables forming the model input. Note that the model input together with the range of validity provides us the **model input space**. This space is the set of all valid values that the model input can take.

¹This holds only if the obstacles and the other MRs are dilated to avoid collisions with the considered MR.

4) **Input-to-object relation:** this is the mapping rule that relates any element within the model input space to a corresponding element within the **object representation space**. In the case of analytical models, this relation can take the form of explicit mathematical equations while in the case of numerical methods, it can take the form of numerical lookup tables or neural networks.

Simplicity is always a desirable property in modelling as it brings tractability, facilitates mathematical analysis, lowers computational requirements, and allows for better problem understanding. One of the fundamental problems in modelling is finding a compromise between simplicity and accuracy that reflects the difference between the behaviour of the mathematical model and the real object. Simple models tend to be highly inaccurate and have reduced ranges of validity; highly accurate models with large ranges of validity tend to be very complex and have little tractability; hence the importance of selecting an adequate level of model complexity. Oversimplification of the model occurs when it is used beyond its range of validity or when variables that have a significant impact on the object representation are disregarded.

Let us analyse this problem in more details by discussing two important consequences of using oversimplified models for robots in the context of CaTP:

1) *Involuntary energy waste*: Oversimplifying the motion-induced energy consumption model when Searching for minimum energy trajectories may significantly degrade performance. This is illustrated with the scenario described in [28], where a rotary-wing UAV (i.e., with propellers and therefore hovering capability) has to collect data from a sensor network. The authors optimize the UAV trajectory to accomplish this task in minimum time and assume that the energy consumed by the UAV is proportional to the time that the UAV spends in the air. In other words, the authors implicitly model the UAV energy consumption as being proportional to the flying time, thus expecting that a real UAV following the trajectory optimized according to the assumed energy model would indeed accomplish its assigned task while draining the minimum energy from its battery.

For those who are unfamiliar with aeronautics or with aerial robotics, the energy model mentioned above might seem reasonable. However, in [29], the authors present an aerodynamic power consumption model for a rotary-wing Unmanned Aerial Vehicle (UAV) that shows that the power consumption also depends on the horizontal speed of the UAV. This model contains a term that increases with the horizontal UAV speed due to the blade's drag. Hence, a UAV executing the minimum time trajectory will travel as fast as possible and consume a large amount of energy instead of minimizing energy consumption.

2) *Unfeasibility of designed trajectory*: another problem of oversimplified models is the possibility of obtaining a trajectory that does not satisfy robot motion constraints. This may lead to collisions with obstacles and among robots as well as failures to perform the planned tasks.

This occurs when the MR's motion model disregards the specific kinematic or dynamic constraints of the MR under consideration.

Let us illustrate this with the following example. Assume that we want to design a trajectory for a car-like MR to pass in a predefined order through a set of points of interest $\{\mathbf{o}_k\}_k^K$ in minimum time. We first model the car-like MR with a single integrator, i.e. the position $\mathbf{p}(t)$ of the robot at time t is described by:

$$\mathbf{p}(t) = \mathbf{p}(0) + \int_0^t \mathbf{v}(\tau) \tau, \quad (1)$$

where $\mathbf{p}(0)$ is the MR's initial position and $\mathbf{v}(\tau)$ is its velocity which can be directly controlled. To make the model more realistic, we take into account the maximum translational speed of the robot, and thus add the following constraint $\|\mathbf{v}(\tau)\|_2 < V_{max}$. According to this model, the optimum trajectory that allows the MR to pass through all the points of interest in minimum time is a piecewise linear path linking consecutive points of interest and requires the MR to use the maximum linear speed possible, V_{max} , at all times.

Following this piece-wise linear path continuously at a constant linear speed without stopping until reaching the end of the path would require, in general, that the MR instantaneously changes direction at each point of interest without stopping. However, this is an impossible manoeuvre for a car-like MR due to its dynamic and kinematic constraints. Its dynamic constraints will not allow abrupt changes in the velocity (whether the change is in direction or in magnitude) and its kinematic constraints will limit the curvature of the turns it can execute. Now, assume that we allow the MR to stop at each point of interest of the piece-wise linear path. This would now require the robot to rotate on the spot at each point of interest to change direction and then continue its path. Yet, this manoeuvre is also impossible for the car-like MR due to its kinematic constraints that are imposed by its own physical geometry.

Clearly, the model (1) used in this example oversimplifies the motion capabilities of the car-like MR. Thus, the solution for the trajectory planning problem derived from such a model results in an unfeasible trajectory for the real car-like MR. Some postprocessing, e.g. smoothing the path, could be done on the resulting trajectory to make it feasible for the real MR, but this would still require considering the MR's kinematic and/or dynamic constraints.

In some cases, increasing the complexity of the MR models may bring only small benefits. For instance, in [30] the authors considered a three wheeled omnidirectional MR and compared two approaches of finding a minimum energy trajectory. The first trajectory was optimized using a certain dynamic model of the robot; the second trajectory used the same dynamic model of the robot, except that it neglected the term accounting for the Coriolis force. Both trajectories were then tested on a real MR. The results showed that when the robot tracked the second trajectory (optimized with the simpler dynamic model),

it consumed just slightly more energy than when it tracked the first one.

As we have explained above, the oversimplification of MR models can have serious consequences, hence the importance of selecting an adequate model complexity. In order to help researchers with no (or little) robotics background, the rest of this section provides a general description of mathematical models describing the motion and energy consumption for two popular MRs: ground wheeled robots and the aerial rotary-wing(s) robots. We will present an overview of the different types of models, their implications, and their limitations. This does not constitute an exhaustive list of all the mathematical models associated with these MRs, but rather an introductory presentation for common models used in trajectory planning. Readers familiar with this research area can skip to section III where we discuss the modelling of communication systems and the wireless channel.

Before moving to the next subsection, we must mention that selecting the appropriate complexity of the models is not always an easy task and sometimes does not have a clear, or even a unique *correct* answer. This is highly dependent on the particular and specific conditions of the problem to be solved. In this tutorial, we aim to raise awareness about the problems related to oversimplification, while underlining that the solution to the latter is not overcomplexification. Indeed, overly complex models might solve some issues due to oversimplification, but may also cause other problems, such as the lack of tractability and the high computational load of the solutions.

A. Wheeled Mobile Robots (WMRs)

We begin this section by quoting the definition of a WMR given in [31]: *A robot capable of locomotion on a surface solely through the actuation of wheel assemblies mounted on the robot and in contact with the surface. A wheel assembly is a device which provides or allows relative motion between its mount and a surface on which it is intended to have a single point of rolling contact.*

WMRs can be implemented in a simple and relatively inexpensive way, making them highly popular for numerous applications, particularly in the context of trajectory planning. They can be classified according to the number of wheels, their type, and spatial configuration within the WMR's frame. These aspects determine the kinematic constraints of the robot. Therefore, before discussing the kinematic model, we briefly present the wheels used in typical WMRs. Some common types are [32]:

- 1) Conventional wheels: these wheels have two degrees of freedom (DOFs), which are rotation around its axis line and rotation around its contact point with the floor.
- 2) Omnidirectional wheels: this is a special type of wheels constructed using a main conventional wheel and embedded small rollers whose orientation is not aligned with that of the main wheel. This special configuration allows the omnidirectional wheel to operate not only as a conventional wheel, but also to advance along the direction orthogonal to the main wheel's orientation.

These wheels can be actuated (i.e., mechanically directly or indirectly coupled to a motor's shaft).

- 3) Ball wheels: these wheels are, as their name indicates, balls. They can roll in any direction, but they are, in general, unactuated (as opposed to omnidirectional wheels which can be actuated).

Kinematics is the field of mechanics that studies the motion of objects without considering the effect of forces. WMR kinematic models describe the relation between the angular speed of the WMR's actuated wheels and the velocity of the WMR's object representation, i.e., the translational and angular velocities of \mathbf{p} . There are two types of kinematic models: the forward kinematic model and the inverse kinematic model. Forward kinematic models describe the WMR's velocities in terms of the angular speeds of the wheels, i.e. the wheels' angular speeds are the model's inputs and the WMR's velocities are the model's output. Inverse kinematic models describe the opposite relation: the WMR's velocities are the model's inputs, and the angular speeds of the wheels are the model's outputs. The forward kinematic model is useful for analyzing the movement of the WMR generated by a particular control signal applied to its motors. The inverse kinematic model is useful to make the WMR's controller track a desired trajectory (i.e. the model's input is the desired trajectory and the model's output is the required wheels' angular speeds).

In the following sections, we will discuss the above-mentioned kinematic models for various WMRs.

1) *Forward Kinematic Model:* As mentioned before, although WMRs are not single points in the plane, but rather systems that cover a certain area, their object representation consists of their horizontal position \mathbf{p} and orientation ϕ (WMRs usually operate in 2D). The point \mathbf{p} is a point on the WMR's frame whose exact location is selected to facilitate kinematic and dynamic analysis. For instance, in the TOMR of Fig. 2 the point \mathbf{p} is chosen to be the geometrical center of the MR, but in the DDR, the point \mathbf{p} is the center of the axis-line of the actuated wheels, rather than the geometrical center of the robot, see Fig. 1. Other choices for \mathbf{p} are also possible, but these would complicate the mathematical analysis of the motion models.

The type of each wheel and their location within the WMR's frame determines the forward kinematic model. Each type of wheel imposes different constraints. For instance, a conventional wheel is allowed for rotational slippage around its contact point with the floor, but is not allowed for translational slippage. The key hypotheses in the kinematic model derivation are the following: (i) the WMR's frame is solid and suffers no deformation; (ii) all the wheels are in contact with the floor at all times, which implies the consideration of a flat floor; (iii) each wheel is in contact with the floor only at a single point. For more details about the derivations of forward kinematic models, the interested reader can consult [32].

We begin with the unicycle, which is the simplest WMR. It has a single steerable actuated wheel whose orientation w.r.t. to the x axis is θ and its ground contact point is $[x, y]$. The

kinematic model of the unicycle is [33]:

$$\begin{bmatrix} \dot{x} \\ \dot{y} \\ \dot{\theta} \end{bmatrix} = \begin{bmatrix} \cos(\theta) \\ \sin(\theta) \\ 0 \end{bmatrix} v + \begin{bmatrix} 0 \\ 0 \\ 1 \end{bmatrix} \omega, \quad (2)$$

where $v \geq 0$ is the driving velocity and ω is the steering velocity.

The bicycle is a vehicle that has a back conventional wheel and a front steerable conventional wheel. The back wheel's ground contact point is $[x, y]$, the orientation of the vehicle w.r.t. the x axis is θ , and the front wheel's orientation w.r.t. to the vehicle is ϕ . If the driving wheel is the front wheel and the backwheel is unactuated, then the bicycle kinematic model is [33]:

$$\begin{bmatrix} \dot{x} \\ \dot{y} \\ \dot{\theta} \\ \dot{\phi} \end{bmatrix} = \begin{bmatrix} \cos(\theta) \cos(\phi) \\ \sin(\theta) \cos(\phi) \\ \sin(\phi)/\ell \\ 0 \end{bmatrix} v + \begin{bmatrix} 0 \\ 0 \\ 0 \\ 1 \end{bmatrix} \omega, \quad (3)$$

where L is the distance between the center of both wheels. Alternatively, if the back wheel is the one driving the vehicle and the front wheel is unactuated, then the kinematic model is [33]:

$$\begin{bmatrix} \dot{x} \\ \dot{y} \\ \dot{\theta} \\ \dot{\phi} \end{bmatrix} = \begin{bmatrix} \cos(\theta) \\ \sin(\theta) \\ 0 \\ \tan(\phi)/\ell \end{bmatrix} v + \begin{bmatrix} 0 \\ 0 \\ 0 \\ 1 \end{bmatrix} \omega. \quad (4)$$

Note that the model (4) is not valid for $\phi = \pm\pi/2$.

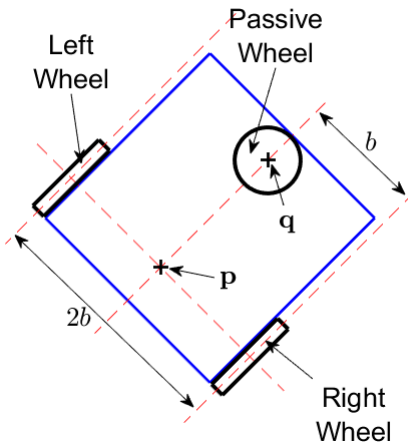


Figure 1. Differential Drive robot diagram.

Now, we consider the DDR, see Fig. 1. This robot has two conventional wheels, of radii r , which are actuated by separate motors. The horizontal position of the DDR is determined by the point p located in the center of the line linking the points of contact of both wheels with the floor. The distance between these points is $2b$. A third unactuated wheel making contact with the floor at point q provides mechanical stability; it is chosen so that it does not impose any kinematic constraints. The corresponding kinematic model for the DDR is [34]:

$$\begin{bmatrix} \dot{x} \\ \dot{y} \\ \dot{\theta} \end{bmatrix} = \frac{r}{2} \begin{bmatrix} \cos(\theta) & \cos(\theta) \\ \sin(\theta) & \sin(\theta) \\ \frac{1}{b} & -\frac{1}{b} \end{bmatrix} \begin{bmatrix} \omega_R \\ \omega_L \end{bmatrix}, \quad (5)$$

where $\omega_R \in \mathbb{R}$ and $\omega_L \in \mathbb{R}$ are the angular speeds of the right and left wheels, x and y are the x and y positions of the DDR, and θ is its orientation. The model input vector in (5) is two dimensional, while the DDR configuration (i.e. the output vector) is three dimensional. This implies that the DDR translational velocity (i.e. $[\dot{x}, \dot{y}]$) and its angular speed $\dot{\theta}$ cannot be controlled independently. The DDR translational speed (i.e. the magnitude of the DDR translational velocity) and its angular speed are expressed as:

$$\begin{bmatrix} v \\ \dot{\theta} \end{bmatrix} = \frac{r}{2} \begin{bmatrix} 1 & 1 \\ 1 & -1 \end{bmatrix} \begin{bmatrix} \omega_R \\ \omega_L \end{bmatrix}. \quad (6)$$

Note that the DDR model can also be modelled by the unicycle's kinematic model (2). To see this, let $[x, y]$ in (2) represent the middle point in the axis linking both wheels (i.e., p in Fig. 1) of the DDR. Then, we combine the expressions for the angular and translational speeds (6) with (2). This results in the DDR kinematic model (5). Hence, the DDR can be considered as a *virtual unicycle*. The difference between representing the DDR with (5) and with (2) is that the first models the DDR motion as a function of the wheels' speed, while the other models the DDR motion as a function of its angular and translational speeds.

The car-like robot has two rear conventional wheels which are mechanically coupled to the same motor, and also has two conventional steerable front wheels which mechanically coupled. The kinematic model of this WMR is [35]:

$$\begin{bmatrix} \dot{x} \\ \dot{y} \\ \dot{\theta} \end{bmatrix} = \omega r \begin{bmatrix} \cos\left(\frac{\pi}{2} - \theta\right) \\ \sin\left(\frac{\pi}{2} - \theta\right) \\ \frac{1}{L} \tan(\delta) \end{bmatrix}. \quad (7)$$

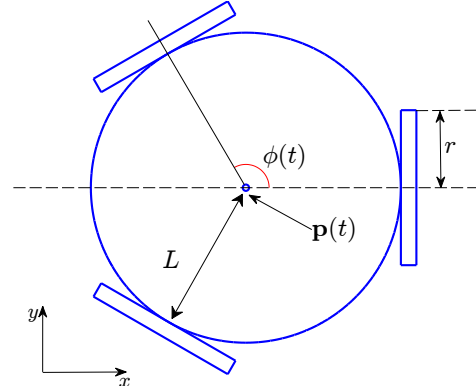


Figure 2. Three wheeled omnidirectional robot diagram.

Just as the DDR can be considered a *virtual unicycle*, the car-like robot can also be considered as a *virtual bicycle* [33] and can be modelled as such.

Another common class of WMR includes omnidirectional robots. They have the particularity of using omnidirectional wheels that enable the robot's omnidirectional motion, i.e., moving in any direction at any time. One popular MR be-

longing to this class is the three wheeled omnidirectional MR, see Fig. 2. Its kinematic model is [36]:

$$\begin{bmatrix} \dot{x} \\ \dot{y} \\ \dot{\phi} \end{bmatrix} = r \begin{bmatrix} 0 & 1 & L \\ -\sin\left(\frac{\pi}{3}\right) & -\cos\left(\frac{\pi}{3}\right) & L \\ \sin\left(\frac{\pi}{3}\right) & -\cos\left(\frac{\pi}{3}\right) & L \end{bmatrix}^{-1} \begin{bmatrix} \omega_1 \\ \omega_2 \\ \omega_3 \end{bmatrix}, \quad (8)$$

where r is the radii of the omnidirectional wheels, ω_i is the angular speed of the i th wheel, and L is the distance from the wheels to the robot's center. Unlike the kinematic models of DDR and CLR, that of the three wheeled omnidirectional MR is fully invertible analytically. Hence, we can always determine independently the translational velocity and the angular speed of the MR and find the corresponding exact angular speed of each wheel. Therefore, the three wheeled omnidirectional MR does not present any kinematic restriction on its motion, but dynamic constraints still need to be considered, as it will be described in section II-A3.

2) *Inverse Kinematic Model*: As explained in the previous section, the forward kinematic model is obtained by analysing the MR's geometry and applying the motion constraints imposed by the wheels. The inverse kinematic models are obtained by inverting the forward kinematic model.

In some cases, the derivation of the inverse kinematic model is straightforward. For instance, consider the kinematic model of the three-wheeled omnidirectional MR (8). This is a linear model involving an invertible matrix; thus, the inverse kinematic model for the three-wheeled omnidirectional MR is:

$$\begin{bmatrix} \omega_1 \\ \omega_2 \\ \omega_3 \end{bmatrix} = \frac{1}{r} \begin{bmatrix} 0 & 1 & L \\ -\sin\left(\frac{\pi}{3}\right) & -\cos\left(\frac{\pi}{3}\right) & L \\ \sin\left(\frac{\pi}{3}\right) & -\cos\left(\frac{\pi}{3}\right) & L \end{bmatrix} \begin{bmatrix} \dot{x} \\ \dot{y} \\ \dot{\phi} \end{bmatrix}, \quad (9)$$

Similarly, the inverse kinematic model for the DDR can be derived from inverting (6):

$$\begin{bmatrix} \omega_R \\ \omega_L \end{bmatrix} = \frac{b}{r} \begin{bmatrix} \frac{1}{b} & 1 \\ \frac{1}{b} & -1 \end{bmatrix} \begin{bmatrix} v \\ \dot{\phi} \end{bmatrix}, \quad (10)$$

Finally, some MRs have complex forward kinematic models that are difficult to invert analytically due to nonlinearities and singularities. In such cases, alternatives for the derivation of the inverse kinematic model are based on machine learning techniques [37].

3) *Dynamic Model*: Dynamic models consider the forces exerted by the robot on its environment. They relate the WMR motion to the torque exerted by each motor and the electric signals producing it. WMR can be modelled as a nonlinear dynamic system whose general form is [38]:

$$\dot{\mathbf{z}} = f(\dot{\mathbf{z}}, \mathbf{u}), \quad (11)$$

where \mathbf{z} is the *state vector* of the WMR²; \mathbf{u} is the input signal vector and $f(\cdot)$ is a general function which can be linear or non-linear.

Let us begin the discussion of dynamic models with the popular *pure integrator model*:

$$\frac{d^n \mathbf{p}(t)}{dt^n} = \mathbf{u}(t), \quad n \in \mathbb{N}^+, \quad (12)$$

²The state vector is a vector composed of a set of state variables. Broadly speaking, a set of state variables is the minimum set of variables required (in addition to the input) to uniquely determine the state vector. For more information on the subject, see [38].

where \mathbf{u} is the control signal and \mathbf{p} is the WMR position. (12) models a generic omnidirectional robot. It is also a very popular model due to its simplicity, which eases the theoretical analyses. This allows analytical results to be derived with less effort than with the use of more elaborated dynamic models (at the expense of accuracy, however). To make (12) more realistic, while slightly increasing the complexity, we can bound the control signal as $\|\mathbf{u}\|_2 \leq u_{max}$ or $\|\mathbf{u}\|_\infty \leq u_{max}$, etc.

Now, we discuss the order n in the model (12). If $n = 1$, we obtain the *single integrator model*, which allows for abrupt velocity changes. This model can describe with some accuracy the WMR motion under any of the following conditions: (i) the WMR speed is constant or changes slowly; (ii) the WMR dynamics is fast enough to follow the input. For instance, in [22] the authors used this model to design trajectories, which were then tested experimentally on real WMRs.

The model (12) with $n = 2$, which is referred to as the *double integrator model*, limits the WMR acceleration. It is also a very common model in mobile robotics [5], [39].

The *pure integrator model* is a very simple general model used to describe a variety of WMRs, but greatly lacks accuracy. We will now begin to discuss more complex and specific dynamic models.

Most WMRs use DC motors to drive their wheels [34] as they are cheap, easy to control, and efficient. The WMR's dynamic model can be derived by first modeling the DC motor and then by combining the motor models considering the MR frame. Following such a procedure, a dynamic model for the DDR is found to be [34]:

$$\dot{\mathbf{z}} = \mathbf{A}\mathbf{z} + \mathbf{B}\mathbf{u}, \quad (13)$$

$$\dot{\mathbf{p}} = \begin{bmatrix} \cos(\phi) & \sin(\phi) & 0, \\ 0 & 0 & 1, \end{bmatrix}^T \mathbf{z}, \quad (14)$$

$$\mathbf{z} = \mathbf{T}_q \begin{bmatrix} \omega_R \\ \omega_L \end{bmatrix}, \quad (15)$$

$$\mathbf{T}_q = \frac{r}{2} \begin{bmatrix} 1 & 1 \\ b^{-1} & -b^{-1} \end{bmatrix}, \quad (16)$$

$$\mathbf{p} = [x, y, \phi]^T, \quad (17)$$

$$\mathbf{z} = [v, \dot{\phi}]^T, \quad (18)$$

$$\mathbf{u} = [u_R, u_L]^T, \quad (19)$$

where u_R and u_L are the normalized input DC voltage to the motors and so $|u_R| \leq 1$ and $|u_L| \leq 1$; ω_R and ω_L are the angular speeds of the right and left wheels, respectively; \mathbf{p} is the pose of the WMR (i.e., the WMR's horizontal position and orientation), v and $\dot{\phi}$ are the translational speed and the angular speed (around its center) of the WMR, respectively. The matrices \mathbf{A} and \mathbf{B} contain information related to the inertia of the MR, its weight, the friction, the battery voltage level, and other electromechanical parameters of the used motors.

From this dynamic model we observe that:

- 1) The DDR's state vector \mathbf{z} is linear w.r.t. the control input \mathbf{u} , see (13), but the pose is nonlinear w.r.t. the state, see (14).

2) The DDR's velocity, encoded in \mathbf{z} , is related to the input \mathbf{u} by a first-order linear system and its pose is related to \mathbf{u} by a second-order nonlinear system. This implies that the input \mathbf{u} controls the DDR's acceleration, and so the state \mathbf{z} cannot change abruptly. As a consequence, the WMR has the following limitations: (i) it cannot change the speed abruptly, thus requiring a non-zero deceleration time to stop; (ii) it cannot change direction abruptly.

3) If $\dot{\mathbf{z}}$ in (13) is significantly small, then $\mathbf{z} \approx -\mathbf{A}^{-1}\mathbf{B}\mathbf{u}$. In other words, if the DDR's acceleration is significantly small, then the WMR state \mathbf{z} almost becomes linear w.r.t. the control signal \mathbf{u} . As such, the dynamic DDR motion model (13)-(17) does not add additional constraints and can be sufficiently modelled by the kinematic model.

The dynamic model of the three-wheel omnidirectional MR is [30]:

$$\dot{\mathbf{z}} = \mathbf{A}(\phi, \dot{\phi})\mathbf{z} + \mathbf{B}\mathbf{u}, \quad (20)$$

$$\mathbf{p} = [\mathbf{I}_{3 \times 3} \quad \mathbf{O}_{3 \times 3}] \mathbf{z}, \quad (21)$$

$$\mathbf{z} = [x, y, \phi, \dot{x}, \dot{y}, \dot{\phi}]^T, \quad (22)$$

$$\mathbf{u} = [u_1, u_2, u_3]^T, \quad (23)$$

where:

$$\mathbf{A}(\phi, \dot{\phi}) = \begin{bmatrix} \mathbf{O}_{3 \times 3} & \mathbf{I}_{3 \times 3} \\ \mathbf{O}_{3 \times 3} & \mathbf{R}(\phi)\dot{\mathbf{R}}^T(\phi)\dot{\phi} - \mathbf{C} \end{bmatrix}, \quad (24)$$

$$\mathbf{R}(\phi) = \begin{bmatrix} \cos(\phi) & -\sin(\phi) & 0, \\ \sin(\phi) & \cos(\phi) & 0, \\ 0 & 0 & 1, \end{bmatrix}, \quad (25)$$

The matrices \mathbf{B} and \mathbf{C} in (20) and (24), respectively, depend on the electromechanical characteristics of the particular three-wheel omnidirectional MR. The matrix $\mathbf{R}(\phi)\dot{\mathbf{R}}^T(\phi)\dot{\phi}$ is related to the Coriolis force.

As opposed to the DDR, where the dynamic model described in (13) is linear, the three-wheel omnidirectional MR dynamic model in (20)-(25) is nonlinear w.r.t. the input. The nonlinearity comes from $\mathbf{A}(\phi, \dot{\phi})$, and in particular from the component $\mathbf{R}(\phi)\dot{\mathbf{R}}^T(\phi)\dot{\phi}$ in (22) which is produced by the Coriolis force.

After having discussed some dynamic models for WMRs, we now discuss the models used for describing their energy consumption due to motion.

4) *Energy Consumption model:* Most MRs draw their energy from a battery. Due to the limited capacity of the battery, it is important to calculate the MR energy consumption to determine their operation time. There are various approaches to derive energy consumption models, but we will discuss only some of the most common ones.

1) **Electric model.** Most WMRs use DC motors to actuate their wheels because of their advantages in comparison to other types of motors, as explained in [34]. In this approach, we first calculate the energy consumed by the k th motor as a function of the instantaneous electric power:

$$E_k = \int_t p_k(t) dt, \quad (26)$$

$$p_k(t) = i_k(t)v_k(t), \quad (27)$$

where $p_k(t)$ is the instantaneous electric power consumed by the k th motor, $i_k(t)$ is the input current, and $v_k(t)$ is the DC input voltage to the k th motor. Since this is a DC motor, the input variable which controls it is the DC input voltage (controlled using PWM), which is given as:

$$v_k(t) = u_k(t)V_s, \quad (28)$$

where V_s is the amplitude of the PWM signal and $u_k(t) \in [-1, 1]$ is the normalized control signal. Circuit theory and electromechanical equations are then used to derive the equations relating the input current $i_k(t)$ to the angular speed ω_k of the wheel which is mechanically coupled with the motor's shaft. Then, the dynamic model is used to relate the WMR state vector to the wheel's angular speed. Finally, these equations are combined to obtain an equation relating the WMR energy consumption to the input vector \mathbf{u} and the WMR state vector. To illustrate this method, we briefly present the energy consumption models of a DDR and of a TOMR. According to [40], the DDR's energy consumption model is:

$$\begin{aligned} E &= \int_t \mathbf{i}^T(t)\mathbf{v}(t)dt, \\ &= V_s \int_t \mathbf{i}^T(t)\mathbf{u}(t)dt, \\ &= \int_t (k_1 \|\mathbf{u}(t)\|^2 - k_2 \mathbf{z}^T(t)\mathbf{T}_q^{-T}\mathbf{u}(t)) dt, \end{aligned} \quad (29)$$

where the parameters k_1 and k_2 depend on electromechanical properties of the motors. Variables \mathbf{u} , \mathbf{z} and \mathbf{T}_q have the same definition as in (13)-(17). The energy consumption model for the three-wheel omnidirectional MR is given in [30] as:

$$\begin{aligned} E &= \int_t \mathbf{i}^T(t)\mathbf{v}(t)dt, \\ &= V_s \int_t \mathbf{i}^T(t)\mathbf{u}(t)dt, \\ &= \int_t (k_1 \|\mathbf{u}(t)\|^2 - k_2 \mathbf{p}^T(t)\mathbf{R}(\phi)\mathbf{B}\mathbf{u}(t)) dt, \end{aligned} \quad (30)$$

where $\mathbf{u}(t)$, $\mathbf{p}(t)$, and \mathbf{T}_q have the same definition as in (20), while k_1 and k_2 depend on the motor's electromechanical characteristics. In [41], the authors present an energy consumption model for a car-like robot derived using the same method, but neglecting the energy required to steer.

This model describes the electrical energy consumed at the input of the motors and takes into account the energy lost as heat within the motor. Note that (29) and (30) are quadratic functions of the normalized control signal $\mathbf{u}(t)$.

2) **Physics approach.** Another approach to describe the WMR energy consumption is to analyze the system from an external perspective and calculate the WMR's kinetic energy and the energy required to overcome the floor's friction. To illustrate this type of model, let us consider

the energy consumption model of the DDR presented in [42]:

$$E_{motors} = E_{kin} + E_{res}, \quad (31)$$

where E_{kin} is the kinetic energy, E_{res} is the energy consumed by the motors to overcome the traction resistance presented by the friction of the floor, and E_{motors} is the energy consumed by the motors which is *observable* from an external point of view, i.e., without taking into account the internal losses. The kinetic energy is given by:

$$\begin{aligned} E_{kin} &= \frac{1}{2}mv^2(t) + I\omega^2(t), \\ &= \int_t \{mv(t)a(t) + I\omega(t)\beta(t)\}dt, \end{aligned} \quad (32)$$

where m is the total WMR's mass; I is the total WMR's rotational inertia; v and ω are the translational and rotational speeds; $a(t)$ and $\beta(t)$ are the translational and rotational accelerations. Note that the products $v(t)a(t)$ and $\omega(t)\beta(t)$ in (32) can be negative when the WMR stops. This means that the WMR's motors get back some power that **could** be recovered by the WMR's electrical system. However, most WMR's do not have the electric systems needed to recover such power and thus, considering this limitation, (32) becomes:

$$E_{kin} = \int_t \{m \max(v(t)a(t), 0) + I \max(\omega(t)\beta(t), 0)\}dt. \quad (33)$$

The term describing the energy consumed to overcome friction in (31) is:

$$E_{res} = 2\mu mg \int_t \max(|v(t)|, b|\omega(t)|)dt. \quad (34)$$

Note that $\int_t |v(t)|dt$ is approximately the distance travelled by the DDR. The advantage of this model is that it is independent of the type of motor used by the WMR, and it requires only the mass m and the rotational inertia I of the WMR which can be estimated. The disadvantage is that it only considers the energy expenditure observed from the outside and does not take into account the internal losses of the motors and the circuitry.

3) **Data driven Model.** The energy consumption models mentioned above are derived from physical principles. Those theoretical models, for the sake of tractability, often ignore certain effects, such as nonlinearities of the motor or the influence of temperature on the electric resistances. Another approach consists of measuring the electric consumption of the WMR under different conditions, creating a dataset, and then training numerical models. The authors of [43] present a simple implementation of this approach by measuring the power consumed by DC motors at different angular speeds. The authors note that a suitable model for the power consumption of the k th motor is:

$$P_k = \sum_{j=0}^6 a_j \omega_k^j, \quad (35)$$

where ω_k is the angular speed of the k th motor and $\{a_j\}_{j=0}^6$ are experimentally determined coefficients. The model in (35) is then combined with the kinetic model, which relates the velocity of the WMR to the angular speed of the wheels ω_k , to obtain the power consumed by the WMR. After integration over time, we obtain the consumed energy.

In [44], there are two examples of this type of energy consumption models. First, the authors measure the power consumption of the PPRK (a commercial three-wheeled omnidirectional MR) moving at a constant linear speed v . The measurements are done at different linear speeds up to a maximum value. After a numerical analysis of the measurements, the authors observed that the power consumed by the PPRK can be well modelled by a fourth order polynomial function of the linear speed:

$$P_{PPRK} = \sum_{j=0}^4 a_j v^j, \quad (36)$$

where $\{a_j\}_{j=0}^4$ are the fitted coefficients. According to the measurements, for low speeds, the energy consumption is an affine function of the linear speed v . Next, the authors did the same for the Pioneer 3DX (a commercial DDR) and measured its energy consumption while moving at constant speed on a straight line. Due to limitations in the robot's internal system, the Pioneer 3DX could not be operated at its maximum linear speed. The experimental results showed that the power consumption of this robot can be modelled with an affine function of the linear speed:

$$P_{3DX} = \sum_{j=0}^1 a_j v^j. \quad (37)$$

The derivation of this type of model can require significant time to gather data in the laboratory. Additionally, the generalisation of the derived models to conditions different from those of the modeling phase might exhibit an uncertain accuracy, e.g. when trying to use the model in (37) to predict the energy consumption of the Pioneer 3DX while moving along curves or at variable linear speed. On the other hand, one advantage of this type of model is that they do not require deep theoretical knowledge. Also, they can implicitly consider the various complex processes involved in energy consumption, which may be complicated to take into account in the theoretical models. For example in [43], the authors mention that from electromagnetic theory, DC motors can be modelled with a second-order polynomial of the angular speed ω . Yet, measurements show that such a model is insufficient; for example, the sixth-order polynomial model introduced in (35) exhibited a much better fit on real measurements. This may be due to the fact that the second-order model derived from theory overlooks certain processes, while the model in (35) took them into account implicitly through the fitting process.

4) **Restricted Domain Models.** Some simple energy consumption models are derived from more complex models by constraining their range of validity. To illustrate this, let us consider the work in [45] where the authors use an electric energy consumption model for a DDR, similar to the one used in (29). They restrict the DDR to move within a straight line with a trapezoidal linear speed profile. For such a trajectory, they calculate analytically the energy consumption starting from the electric energy consumption model and obtain the following expression:

$$E = \sum_{j=-1}^3 a_j \omega^j, \quad (38)$$

where ω is the angular speed of the DDR wheels. The model (38) exposes an interesting phenomenon that is sometimes overlooked: motors can be inefficient when operated at very low speeds; as the motor's speed decreases the term ω^{-1} in (38) dominates the energy consumption and grows very quickly. After the optimization of the trapezoidal speed profile, the authors found that the energy consumption is proportional to the distance travelled when the total duration of movement remains constant. Based on the result in (38), the authors of [46] modeled the energy consumption as being proportional to the distance travelled by the WMR, D :

$$E = kD, \quad (39)$$

where k is a proportionality factor. The model (39) has been adopted by many authors for simplicity and is sometimes derived in a similar manner in different papers or sometimes just assumed because it is *intuitive* and simple; see for example [47] and [48].

In [49], the authors rewrote the model (39) as:

$$E \propto \int_t |v(t)| dt, \quad (40)$$

These types of models are, in general, simplifications of other more complex models under certain conditions. When choosing a model, we must take into consideration where it comes from and how it was derived in order to see if the application in which we intend to use it is close enough to the conditions under which the model was derived, so as to make sure that we do not operate the model outside its range of validity. Otherwise, if we neglect this aspect, then the model selected might deviate significantly from the true energy consumption. For example, while the model introduced in (39) is appropriate when a WMR is moving at a constant speed, it may be quite inaccurate when the speed of the varies considerably over time.

5) **Square norm.** Finally, another popular approach within the control theory community is to assume that the energy consumption is given by:

$$E = \int_0^t \|\mathbf{u}(\tau)\|^2 \tau, \quad (41)$$

where \mathbf{u} is the control signal of the WMR dynamic model. This is notably a simplification of the energy

consumption models derived through circuit theory presented in (29) and (30). The model in (41) becomes closer to the models (29) and (30) when the WMR operates at low speeds and/or the coefficient k_2 of those models is small.

Although motion consumes a significant part of the energy in WMRs, there are also other processes which consume a non-negligible amount of energy. In [50], the authors empirically evaluated the contribution of different processes to the energy consumption of a DDR and found that the sensors and microcontrollers also contribute significantly to energy consumption. The microcontroller's power consumption can be modelled as constants, since they usually perform low level tasks which are repetitive and relatively stable. On the other hand, the power consumption of the embedded computers can be modelled as a stochastic process as they usually perform tasks which depend more on exogenous inputs, and thus have a more variable behaviour.

B. Rotary-wing UAVs

The study of the motion of aerial vehicles is a complex subject that has been investigated since the early appearance of the first airplanes. There is a large body of literature on the aerodynamic aspects of these vehicles and their modeling. In this section, we will discuss the quadrotor aerial robot, which is a basic type of multirotor UAV.

Multirotor aerial robots (also called rotary-wing aerial robots) are one of the most popular types of aerial robots nowadays. One of the most common type of these UAVs is the quadrotor, which is the subject of this section.

The WMRs discussed in the previous section operate in 2D and their configuration is fully described by their horizontal position and orientation. In contrast, UAVs operate in 3D. To fully describe their configuration, we need to specify their 3D position, as well as their attitude³, which can be expressed using either Euler angles or quaternions [51], [51]. In this tutorial, we will limit the discussion to models representing the attitude using Euler angles; details about the utilisation of quaternions to represent the attitude can be found in [52].

The configuration of the UAV can be described using Euler angles as:

$$\mathbf{p}(t) = [x, y, z]^T, \quad (42)$$

where $[x, y, z]^T$ is the UAV center of mass and θ , ϕ , and ψ are the Euler angles of roll, pitch, and yaw, respectively, which describe the orientation of the UAV; see [53] for a more detailed geometrical description of these angles. Note that $[x, y, z]^T$ is represented in a static coordinate frame attached to the world and not to the UAV itself, and $[\theta, \phi, \psi]^T$ are represented in a coordinate frame attached to the center of mass of the UAV oriented in the same manner as the inertial coordinate frame. Before discussing the quadrotor dynamic model, we will briefly discuss the physical principles that allow it to fly. In a classic quadrotor, the four propellers lie in the same plane and are oriented vertically. When the propeller

³The attitude, not to be confused with the altitude, is the equivalent of the orientation for the ground WMRs.

rotates, it creates thrust in the same direction as its orientation and with a sense opposing the gravity. The faster the propeller turns, the larger the thrust generated. When all four propellers produce the same thrust, the plane containing all four propellers is parallel to the floor and the resulting thrust is vertical. If this thrust equals the gravity force, then the quadrotor remains in the air hovering. When one propeller turns faster or slower than the other, the quadrotor tilts and the resulting thrust presents a horizontal component, making the UAV move in the horizontal plane.

Just as the dynamic models of the WMRs were derived starting from the electrical analysis of their motors, the derivation of the dynamic model for multirotors begins in the same way. Consider a dynamic model for the quadrotor that is used by many roboticists [54]:

$$\begin{bmatrix} \frac{d^2x}{dt^2} \\ \frac{d^2y}{dt^2} \\ \frac{d^2z}{dt^2} \end{bmatrix} = \begin{bmatrix} c(\phi)s(\theta)c(\psi) + s(\phi)s(\psi) \\ c(\phi)s(\theta)s(\psi) - s(\phi)c(\psi) \\ c(\phi)c(\theta) \end{bmatrix} \frac{u_z}{m} - \begin{bmatrix} 0 \\ 0 \\ g \end{bmatrix}, \quad (43)$$

$$\begin{bmatrix} \frac{d^2\phi}{dt^2} \\ \frac{d^2\theta}{dt^2} \\ \frac{d^2\psi}{dt^2} \end{bmatrix} = \begin{bmatrix} \left(\frac{I_y - I_z}{I_x}\right) \frac{d\theta}{dt} \frac{d\psi}{dt} - \frac{J}{I_x} \frac{d\theta}{dt} q_w \\ \left(\frac{I_z - I_x}{I_y}\right) \frac{d\phi}{dt} \frac{d\psi}{dt} + \frac{J}{I_y} \frac{d\phi}{dt} q_w \\ \left(\frac{I_x - I_y}{I_z}\right) \frac{d\phi}{dt} \frac{d\theta}{dt} \end{bmatrix} + \begin{bmatrix} \frac{\ell u_y}{I_x} \\ \frac{\ell u_x}{I_y} \\ \frac{u_\psi}{I_z} \end{bmatrix}, \quad (44)$$

$$\begin{bmatrix} u_x \\ u_y \\ u_z \\ u_\psi \end{bmatrix} = \begin{bmatrix} -\kappa_b & 0 & \kappa_b & 0 \\ 0 & \kappa_b & 0 & -\kappa_b \\ \kappa_b & \kappa_b & \kappa_b & \kappa_b \\ \kappa_\tau & -\kappa_\tau & \kappa_\tau & -\kappa_\tau \end{bmatrix} \begin{bmatrix} \omega_1^2 \\ \omega_2^2 \\ \omega_3^2 \\ \omega_4^2 \end{bmatrix}, \quad (45)$$

$$q_w = \omega_1 - \omega_2 + \omega_3 - \omega_4, \quad (46)$$

where $u_x(t)$, $u_y(t)$, $u_z(t)$, and $u_\psi(t)$ denote the control signals for the drone; $\omega_j(t)$ is the angular velocity of the j th motor; m is the total mass of the drone, g is the gravitational constant; ℓ is the distance from the center of the quadrotor to each motor; I_x , I_y , and I_z are the rotational inertia components; J is the total inertia of the motors; and κ_b and κ_τ are the thrust and aerodynamic drag factors of the propellers. Note that the matrix relating the vector inputs $[u_z \ u_y \ u_x \ u_\psi]^T$ with the square angular velocities vector $[\omega_1^2(t) \ \omega_2^2(t) \ \omega_3^2(t) \ \omega_4^2(t)]^T$ is not singular.

Equation (44) describes the drone's Euler angles (roll (ϕ), pitch (θ), and yaw (ψ)) measured with respect to the axes o_Bx_B , o_BY_B , and o_Bz_B , with $(o_Bx_BY_Bz_B)$ being the body axis system whose origin o_B is given by the geometric centre of the quadrotor.

The quadrotor motion given by the model in (43)-(46) is described w.r.t. to a fixed orthogonal axis set ($oxyz$), where oz points vertically up the gravity vector $[0 \ 0 \ -g]^T$ (earth axes). The origin o is located at a desired height \bar{z} with respect to the ground level. The coordinates x , y , and z in (43) refer to the position of the centre of gravity of the quadrotor in the

space where z is its altitude [55]. In the literature, we find different axis configurations in which the quadrotor motion can be described and each axis configuration provides slightly different models.

The time dependence of the variables in equations (43) and (44) is not explicitly shown in order to lighten the notation. Note also that, due to the symmetry of the quadrotor, we have $I_x = I_y = I$.

More complex models are also possible, which consider external disturbances such as the wind. Regarding the energy consumption of the quadrotor, there are electric models and physics-based models that are derived using approaches similar to those used for the WMR. In [54], the energy consumption of a quadrotor is modeled as:

$$E = \sum_{j=1}^4 \int_t \left[\left(\sum_{k=0}^4 c_k \omega_j^k(t) \right) + c_6 \dot{\omega}_j(t) + c_7 \dot{\omega}_j^2(t) \right. \\ \left. + c_8 \omega_j(t) \dot{\omega}_j(t) + c_9 \omega_j^2(t) \dot{\omega}(t) \right] dt, \quad (47)$$

where the coefficients $\{c_k\}_0^9$ depend on the parameters of the quadrotor's motors and on the geometry of the propellers.

In [56], the authors present the following hybrid energy consumption model, which is based on basic mechanics and completed with some correction factors obtained experimentally:

$$E_c = \int_{t_0}^{t_f} \sum_{j=1}^4 \tau_j(t) \omega_j(t) dt, \quad (48)$$

$$= \int_{t_0}^{t_f} \sum_{j=1}^4 (\dot{\omega}_j(t) + \mathcal{K}_\tau \omega_j^2(t) + D_v \omega_j(t)) \omega_j(t) dt,$$

$$J\dot{\omega}(t) = \tau(t) - \mathcal{K}_\tau \omega^2 - D_v \omega(t) \quad (49)$$

where (48) is the energy consumed by the four motors of the quadrotor. In other words, (48) only describes the amount of energy that is translated into mechanical energy, but disregards the efficiency of the motors. Therefore, to improve (48), the efficiency of the motors (a nonlinear function of the torque and the angular speed) is added. This efficiency term is modeled through laboratory measurements [56]:

$$f_r(\tau, \omega) = a(\omega)\tau^3 + b(\omega)\tau^2 + c(\omega)\tau + d(\omega) \quad (50)$$

where $a(\omega)$, $b(\omega)$, $c(\omega)$, and $d(\omega)$ are second order polynomials of ω whose coefficients are fitted according to experimental measurements. We can then derive a hybrid model combining elements from the data-based models and the physics models presented in the previous section as follows:

$$E_c = \int_{t_0}^{t_f} \sum_{j=1}^4 \frac{(\dot{\omega}_j(t) + \mathcal{K}_\tau \omega_j^2(t) + D_v \omega_j(t)) \omega_j(t)}{f_r(\tau(t), \omega(t))} dt,$$

The advantage of this model is that it only depends on a exogenous variable (i.e., the angular speed of the motors) and not on endogenous variables (i.e., the control signals used).

C. Fixed-wing UAVs

In this section, we briefly discuss fixed-wing UAVs and present a simple, but useful dynamic model for CaTP problems. Fixed-wing UAVs fly using principles that are different from those used by multirotor UAVs and are consequently modelled in a different manner and have different characteristics.

In general, fixed-wing UAVs are more energy-efficient than multirotor UAVs mainly because of their ability to glide. They also fly for longer times, longer distances, and at higher speeds. They are however less agile and cannot land or take-off vertically. As opposed to multirotor UAVs, fixed-wing UAVs are generally not designed to hover. Nevertheless, some special types of fixed-wing UAVs having high thrust-to-weight ratios can hover using complex control techniques [57].

Fixed-wing UAV are controlled by the thrust generated by its propeller(s) and by controlling surfaces (aileron, elevator, and rudder). Micro fixed-wing UAVs usually drive their propellers with an electric motor, while small fixed-wing UAVs can drive it using gas powered motors.

The fixed-wing UAV center of mass position is sometimes described in the North-East-Down (NED) coordinate system, where the down axis points towards the center of the earth and is aligned to the force of gravity. In this case, the altitude is measured in the opposite direction of the down axis. The attitude of the fixed-wing airplane is expressed using Euler angles in the body frame defined as follows: its origin lies in the center of gravity of the airplane, the x axis points to the nose of the plane, the y axis points to the right wing, and the z axis is orthogonal to those two axes and follows the right-hand rule. The roll ϕ describes the rotation about the x axis, the pitch θ describes the rotation about the y axis, and the yaw ψ describes the rotation about the z axis.

The aerodynamics of airplanes are significantly complex and nonlinear. Since this is an elementary tutorial, we will present only a high-level simplified dynamic model that can be used for trajectory planning, as well as one linearized dynamic model. In the absence of wind, a simplified nonlinear dynamic model describing the fixed-wing UAV motion is [58]:

$$\begin{bmatrix} \dot{p}_n \\ \dot{p}_e \\ \dot{h} \end{bmatrix} = V_a \begin{bmatrix} \cos(\psi) \cos(\gamma) \\ \sin(\psi) \cos(\gamma) \\ \sin(\gamma) \end{bmatrix} \quad (51)$$

$$\begin{bmatrix} \dot{\psi} \\ \dot{\gamma} \end{bmatrix} = \begin{bmatrix} \frac{F_{lift} \sin(\phi)}{mV_a} \\ \frac{F_{lift}}{mV_a} \cos(\phi) - \frac{g}{V_a} \cos(\gamma) \end{bmatrix} \quad (52)$$

$$\begin{bmatrix} F_{lift} \\ F_{drag} \end{bmatrix} = \frac{1}{2} \rho V_a^2 S \begin{bmatrix} C_L \\ C_{D_0} + K C_L^2 \end{bmatrix} \quad (53)$$

$$\dot{V}_a = \frac{F_{thrust}}{m} - \frac{F_{drag}}{m} - g \sin(\gamma) \quad (54)$$

where g is the gravitational constant, S is the planform area of the wing, C_{D_0} is the zero lift drag, K is the induced drag factor, m is the mass of the airplane, and ρ is the air density. The input to this model is the lift coefficient⁴ C_L , the thrust

⁴Note that the physical fixed-wing UAV is controlled via its thrust and the three control surfaces (aileron, elevator, and rudder). Hence, even if C_L constitutes the input to the model, in practice it is not directly controlled.

F_{thrust} , and the roll ϕ . \dot{p}_n and \dot{p}_e are the speeds along the north and east axes, respectively, and \dot{h} is the altitude speed measured w.r.t. to the negative direction of the down axis. F_{lift} and F_{drag} are the lift and drag forces experienced by the plane. Finally, V_a is the air speed of the airplane.

The constant altitude and the airspeed scenario (i.e., $\dot{h} = 0$ and $\dot{V}_a = 0$) are common and of particular importance for CaTP applications. In this case, we have $\gamma = 0$, $\dot{\gamma} = 0$, and $F_{thrust} = F_{drag}$. The dynamic model (51) reduces to the kinematic model:

$$\begin{bmatrix} \dot{p}_n \\ \dot{p}_e \end{bmatrix} = V_a \begin{bmatrix} \cos(\psi) \\ \sin(\psi) \end{bmatrix} \quad (55)$$

$$\psi = \frac{g}{V_a} \tan(\phi) \quad (56)$$

Note that (55) is the same model as the unicycle model (2). With this kinematic model, the paths are usually composed of straight lines and circular arcs [59]. The simplified models (51) and (55) are practical, but they do not describe the pitch angle θ . This can be an issue for some CaTP since the variations in the orientation of the antenna mounted on the fixed-wing UAV cannot be fully determined without the pitch θ .

Another simple type of dynamic models for the fixed-wing UAV are the linear models. These models are derived after linearizing more complex nonlinear aerodynamical models around small attitude variations. They are separated into two decoupled models, the longitudinal motion model and the lateral motion model, as follows:

$$\begin{bmatrix} \dot{u} \\ \dot{w} \\ \dot{q} \\ \dot{\theta} \\ \dot{h} \end{bmatrix} = \mathbf{A} \begin{bmatrix} u \\ w \\ q \\ \theta \\ h \end{bmatrix} + \mathbf{B} \begin{bmatrix} \delta_e \\ \tau \end{bmatrix} \quad (57)$$

where τ is the thrust and δ_e is the elevator angle. For the lateral model, we have that:

$$\begin{bmatrix} \dot{v} \\ \dot{p} \\ \dot{r} \\ \dot{\phi} \\ \dot{\psi} \end{bmatrix} = \mathbf{C} \begin{bmatrix} v \\ p \\ r \\ \phi \\ \psi \end{bmatrix} + \mathbf{D} \begin{bmatrix} \delta_a \\ \delta_r \end{bmatrix} \quad (58)$$

where δ_a and δ_r are the action of the aileron and the rudder, respectively. The matrices \mathbf{A} , \mathbf{B} , \mathbf{C} , and \mathbf{D} depend on the particular airplane. Since this is an elementary tutorial, we did not consider the effect of wind on the fixed-wing UAV motion models, but the interested reader can look into [60], [61], [62], [63] for more information regarding this subject.

It can be demonstrated from physical principles that the energy consumption for the fixed-wing UAV can be expressed as follows [10]:

$$E = \int_0^T \left(c_1 \|\mathbf{v}\|^3 + \frac{c_2}{\|\mathbf{v}\|} \left(1 + \frac{\|\mathbf{a}\|^2 - \frac{\mathbf{a}^T \mathbf{v}}{\|\mathbf{v}\|^2}}{g^2} \right) \right) dt \quad (59)$$

$$+ \frac{m}{2} (\|\mathbf{v}\|^2(T) - \|\mathbf{v}\|^2(0)) \quad (60)$$

where \mathbf{v} is the velocity and \mathbf{a} is the acceleration vector of the fixed-wing UAV.

D. Final Comments on Models for Robots

We have presented an overview of some relevant MR's models that are useful for CaTP problems, but have omitted some important observations. The models presented in this section are all in continuous time, but it is possible to transform them into discrete time models by transforming differential equations into difference equations. Continuous-time models allow for the utilisation of many analytical tools based on derivatives, such as calculus of variations. On the other hand, discrete-time models allow for numerical techniques like dynamic programming or other related techniques. It is important to mention that, in practice, the control signals for the ground MRs and the UAVs are executed in digital computers on board, and thus the control system is implemented in discrete time.

Finally, all the kinematic and dynamic models described in this section have an analytical form and are mostly derived from physics. However, there are other types of motion models derived through experimentation and machine learning techniques [64].

III. COMMUNICATIONS SYSTEM

This section mainly addresses researchers who desire to work on CaTP but lack the background in communications systems. Those familiar with the topic can skip this section and directly proceed to section IV.

In this section, we introduce the reader to the basics concepts of communication systems and wireless channel models required to study CaTP problems. We begin by introducing a common communication system: **transceiver**. This is a device composed of a transmitter and a receiver. When a communications link is established between two entities, it can take three different forms:

- 1) **Simplex Link**: one entity operates as a transmitter only and the other operates as receiver only. The data flow is always unidirectional.
- 2) **Full-Duplex Link**: both entities receive and transmit simultaneously. Two independent data flows in opposite directions occur simultaneously.
- 3) **Half-Duplex Link**: both entities receive and transmit in turns, where two independent data flow in opposite directions, but only one is active at a time. This can be implemented using **time duplexing**: during an interval of time, one entity transmits and the other receives, and during the following interval of time, the roles are swapped. This process is periodically repeated.

We now provide a brief overview of the digital transmission. The **source node** generates data as blocks of bits or as a continuous stream of bits. This data is then divided in small groups, which are inserted into packets to form the payload⁵. Each packet has a **header** that contains information such as the destination and/or checkup bits to evaluate the integrity⁶ of the packet at the receiver. There are two main strategies to exploit the checkup bits in the packet's header:

⁵The payload's size can be constant or variable depending on the communications protocol selected.

⁶In other words checking if the packet has been received with errors.

- 1) **Retransmission**: if the receiver does not detect any error in the received data packet, it transmits a confirmation packet back to the source node (containing no payload) indicating that the data packet was correctly received. Thereafter, the source node can transmit new data packets (containing new payload). However, if the receiver detects an error in the received data packet, it does not send back the confirmation packet. When the source node realizes that it did not receive a confirmation packet, it assumes that an error occurred and re-transmits the same data packet. The number of retransmissions will depend on the particular communications protocol.
- 2) **No-retransmission**: if the receiver detects an error in the data packet, it discards the payload. On the other hand, if the packet is correctly received, the receiver does not transmit any confirmation to the source node and simply waits for the next packet. The source node continues to transmit data packets.

The retransmission strategy provides robustness to the transmission of data at the cost of a lowered bit rate and increased latency due to the time spent in confirmation and retransmission of data packets. The no-retransmission strategy can achieve a higher bit rate and lower latency at the cost of more erroneous or missing data. The selection of the transmission strategy will depend on the particular application requirements.

After forming the packets, the transmitter modulates the sequence of bits with a carrier signal of high frequency f_c suitable to be radiated as an electromagnetic waves, which are then radiated through the antenna. The propagation environment modifies the radiated wave before arriving to the receiver's antenna, where it is converted back to an electric signal and processed. The wireless channel model describes the effect that the propagation environment has on the transmitted signal until it reaches the receiver.

A. Wireless channel modelling

In the context of CaTP, oversimplified wireless channel models can lead the designer to overestimate the communications channel quality and to overlook certain channel behaviours that the MR will encounter in real operating conditions. In such cases, the MR might underperform or fail to complete its task due unexpectedly poor communication quality.

To provide the researcher with the *basic* knowledge on communications for CaTP problems, we will limit the discussion to the simplest type of communications systems: narrowband⁷, single-antenna, and single carrier communications systems. In addition, we will not address the issue of interference. The general channel model representing such systems is:

$$y(t) = \mathcal{H}(\mathbf{p}(t), \mathbf{q}(t), t)x(t) + n(t), \quad (61)$$

where $x(t)$ and $y(t)$ are the continuous-time transmitted and received complex signals, respectively; $n(t)$ is the noise generated at the receiver, which is usually modelled as a random complex circular white Gaussian process; $\mathbf{p}(t)$ and $\mathbf{q}(t)$ are

⁷This means that the bandwidth of the modulated signal is significantly smaller than the carrier frequency f_c .

the positions of the transmitter and the receiver, respectively, at time t ; and $\mathcal{H}(\mathbf{p}(t), \mathbf{q}(t), t)$ is the complex channel gain. CaTP problems require models that describe the spatio-temporal channel gain $\mathcal{H}(\mathbf{p}(t), \mathbf{q}(t), t)$. We further discuss different common models to describe the spatial variations of the channel gain.

To model $\mathcal{H}(\mathbf{p}(t), \mathbf{q}(t), t)$, deterministic, stochastic, and machine learning approaches can be used.

1) *Deterministic Models*: In the deterministic approach [65], the wireless channel models are often derived from physical principles. One of the simplest and yet most important channel models is the *power loss model*. It is the base for many more sophisticated channel models. It describes how the mean received signal power varies with the transmitter-receiver distance. It is modelled as [66]:

$$\mathcal{H}(\mathbf{p}(t), \mathbf{q}(t), t) = L_P^{-1}(\mathbf{p}(t), \mathbf{q}(t)), \quad (62)$$

$$L_P(\mathbf{p}(t), \mathbf{q}(t)) = K_0 \left(\frac{d(t)}{d_0} \right)^{\alpha/2}, \quad (63)$$

$$d(t) = \|\mathbf{q}(t) - \mathbf{p}(t)\|_2, \quad (64)$$

where α is the power path loss coefficient, d_0 is a reference distance, and K_0 is the path loss observed at distance d_0 that must be in the far field region [67]. This model is valid for distances larger than d_0 , and is used at distances larger than the radiated signal's wavelength and the physical antenna's dimensions [65]. Under *free space* conditions, the power path loss coefficient becomes $\alpha = 2$, but experimental results have reported path loss coefficients as low as $\alpha = 1.6$ [68], [69] in some urban environments, buildings, and underground mines. This occurs because some hallways and tunnels behave as *giant waveguides* due to their geometry and the presence of metallic objects that act as reflectors.

Experiments have shown that the power path loss coefficient can change after certain distances. This phenomenon is modelled using break points [68] and it extends (63) as follows:

$$L_P(\mathbf{p}(t), \mathbf{q}(t)) = K_0 \left(\frac{d(t)}{d_0} \right)^{\alpha(d(t))/2}, \quad (65)$$

$$\alpha(d) = \begin{cases} \alpha_1, & d < D_{break}, \\ \alpha_2, & d \geq D_{break}, \end{cases} \quad (66)$$

with $\alpha_1 < \alpha_2$ and D_{break} is the breaking point distance [65]. The break point model (65) is more valid over greater distances than the simple power law model (63).

Another deterministic extension to the model in (63), apart from the one in (65), is the two-ray model [66], which takes into consideration only the Line of Sight (LoS) wave and the wave that reaches the receiver's antenna after only one reflection on the floor. This model was originally derived in the context of cellular network communications [70]. It has been tested for scenarios with a transmitter of less than 50m altitude; this model makes the assumption that the distance between the transmitter and the receiver is such that the curvature of the earth can be neglected, and thus the floor is considered flat.

If we consider multiple waves beside the LoS and the reflected wave of the two-ray channel model, then we obtain

the ray tracing model [71], [72], [73]. This method determines the interaction of multiple radiated waves with the environment (e.g., buildings, floor, walls) before arriving to the receiver's antenna and requires a computational map of the area in which both the transmitter and the receiver operate. The accuracy of the ray tracing model increases when the map is more detailed and when more electromagnetic interactions are considered (e.g., reflection, refraction, diffraction). However, this also increases the computational load.

In many cases, a computational map of the region of interest can be difficult and costly to obtain. Indeed, this needs to describe not only the spatial configuration of the objects, but also the electromagnetic properties of the materials such as conductivity, dielectric permittivity, and magnetic permeability. In addition, the computational load of these types of methods can be large as they consider the electromagnetic interactions of the radiated waves with many objects in the environment.

Let us discuss another deterministic channel model which is has been specially devised for indoor operations, and which also requires a map of the building as well as the position of both transceivers. This model draws a straight line between both nodes, counts the number of walls and floors crossed [74], and then represents the losses due to those walls and floors as follows [75]:

$$s(\mathbf{p}(t), \mathbf{q}(t)) = \sum_{k=1}^K WAF(k) + \sum_{j=1}^J FAF(j), \quad (67)$$

where K and J are the number of walls and floors between both transceivers and $WAF(k)$ and $FAF(j)$ are the losses associated to the k th floor and the j th wall, respectively. Note that (67) considers only the losses due to the occlusions caused by walls and floors. Hence, it has to be combined with a power path loss model like (63).

2) *Stochastic Models*: Stochastic models describe the channel in terms of its mean, variance, and correlation functions, rather than trying to predict the exact channel value, unlike deterministic models. Stochastic models are usually simple and can describe the average behaviour of the channel models accurately. Their simplicity allows for mathematical analysis that can provide useful insights in many application domains, including CaTP problems. Using this approach, $\mathcal{H}(\mathbf{p}(t), \mathbf{q}(t), t)$ is modelled as a multi-scale spatial and time-varying stochastic process [76] composed of three terms [76], [77]:

$$\mathcal{H}(\mathbf{p}(t), \mathbf{q}(t), t) = \frac{s(\mathbf{p}(t), \mathbf{q}(t))h(\mathbf{p}(t), \mathbf{q}(t), t)}{L_P(\mathbf{p}(t), \mathbf{q}(t))}, \quad (68)$$

where $s(\mathbf{p}(t), \mathbf{q}(t))$ represents the shadowing [78], [79], $h(\mathbf{p}(t), \mathbf{q}(t), t)$ represents the small-scale fading [67], and $L_P(\mathbf{p}(t), \mathbf{q}(t))$ represents the path loss [66]. We proceed to discuss the physical meaning of these components and their most relevant mathematical models from the perspective of CaTP applications.

- **Path-loss:** this describes a deterministic component that models the mean power loss variations due to distance between the transmitter and the receiver. It usually takes the form of (63). There are also experimentally derived models for the path loss models, such as the Okumura-Hata model [80].

- **Shadowing:** this is a random process that models the signal power reduction due to obstructions caused by large objects⁸, such as buildings. It is a time-invariant term and depends on the transmitter and receiver positions. The shadowing has been experimentally characterized [78] and is generally modelled as a log-normal real random process with variance σ and mean μ . Its spatial autocorrelation has been found experimentally to follow an exponential function [76]⁹:

$$r(d(t)) = \exp(-d(t)/\beta), \quad (69)$$

where β is the decorrelation distance that is usually in the order of 10λ , and is thus also called large-scale fading. For small distances (smaller than β), the shadowing is often considered constant. To give more flexibility to the shadowing model, σ and mean μ can be made dependent on the geographical region [77]. The shadowing effect can thus be simulated numerically using mathematical models [82].

- **Multipath-fading:** the electromagnetic wave radiated by the transmitter reaches the receiver's antenna after travelling through multiple random paths. These multiple components interact with the environment through reflection, diffraction, and refraction before arriving, with different phases, to the receiver's antenna where they are combined. As a consequence, the receiver observes constructive interference in some locations and destructive interference in others. This results in a random spatial process with large signal strength variations over small distances (smaller than one wavelength). This phenomenon is called small-scale fading or multi-path fading [65], [83].

Small-scale fading $h(\mathbf{p}(t), \mathbf{q}(t), t)$ is modelled as a random spatial-temporal process with a certain distribution and spatio-temporal correlations dependent on the environment. The study of small-scale fading is a complex subject. In this elementary tutorial, we focus only on the basic models used in CaTP problems.

Three elements influence $h(\mathbf{p}(t), \mathbf{q}(t), t)$: the position of the receiver $\mathbf{p}(t)$, the position of the transmitter $\mathbf{q}(t)$, and the environment. Any change in any of these elements changes the experienced small-scale fading. In traditional mobile communications, $\mathbf{p}(t)$ and $\mathbf{q}(t)$ are considered uncontrollable time-variant random variables. In that context, $h(\mathbf{p}(t), \mathbf{q}(t), t)$ is considered time variant if the environment varies or if the position of the transceivers changes over time. On the other hand, in CaTP, $h(\mathbf{p}(t), \mathbf{q}(t), t)$ is considered time invariant if $h(\mathbf{p}, \mathbf{q}, t_1) = h(\mathbf{p}, \mathbf{q}, t_2)$ for any $t_1 \neq t_2$ and for any positions \mathbf{p} and \mathbf{q} . In CaTP, the small-scale fading is time-variant only if the environment is dynamic. Otherwise, it is considered time-invariant.

When the small-scale fading is time variant, the temporal variation can be characterized with the coherence time

τ , which indicates the maximum duration over which the small-scale fading term remains almost constant. One common way to model the temporal variation of small-scale fading is as follows: $h(\mathbf{p}, \mathbf{q}, t) = h_k$, for $t \in [k\tau, (k+1)\tau]$ with $\{h_k\}_k$ being a sequence of independent and identically distributed (i.i.d.) random variables. More dynamic environments have shorter coherence times τ . After discussing the concept of time-variance for small-scale fading in the context of CaTP, we now proceed to first discuss time-invariant small-scale fading models, and then briefly discuss time-variant models.

We start with the statistical distribution of small-scale fading. When there is no line of sight between the transceivers nor any particular strong wave due to some reflection, $h(\mathbf{p}, \mathbf{q}, t)$ is commonly modelled as a zero-mean complex circular Gaussian random variable:

$$h(\mathbf{p}, \mathbf{q}, t) = h_R + jh_I, \quad (70)$$

where h_R and h_I are both zero-mean independent real Gaussian random variables with variance $1/2$. Hence, $|h(\mathbf{p}, \mathbf{q}, t)|$ is a Rayleigh distributed random variable, which explains why such a model is referred to Rayleigh fading [67].

Alternatively, if there is a line of sight between both transceivers, then $h(\mathbf{p}, \mathbf{q}, t)$ can be modelled as a non-zero-mean complex circular Gaussian random variable:

$$h(\mathbf{p}, \mathbf{q}, t) = h_R + jh_I + L, \quad (71)$$

where h_R and h_I , which are zero-mean independent real Gaussian random variables with variance $1/2$, represent the ensemble of scattered waves arriving to the receiver's antenna, and L is a real number representing the strength of the line of sight component. The ratio $K = L^2/\text{var}(h_R + jh_I)$ is called the Rician factor. If $K \neq 0$, the distribution of Note that when $K = 0$, we have Rayleigh fading. then we say that we have Rician fading [83] and the norm of $h(\mathbf{p}, \mathbf{q}, t)$ is a random variable with a Rician probability distribution function. There are other common probabilistic distributions used to model $|h(\mathbf{p}, \mathbf{q}, t)|$, such as the Nakagami distribution. Unlike the Rayleigh and the Rician distributions, not all of the other models have physical interpretations, as some distributions are used only because they fit well experimental results.

We now address the modeling of the spatial variations of the small-scale fading. As the name indicates, the magnitude of $h(\mathbf{p}, \mathbf{q}, t)$ varies significantly over very small distances. Many experiments show that the small-scale fading coherence distance is usually lower than $\approx \lambda/2$. There is no universal model to describe its spatial correlation [84], but there is an important theoretical model derived by Jakes [85] for the case where the receiver is surrounded by a ring of uniformly distributed scatterers. In this scenario, the small-scale fading has a Rayleigh distribution and the following normalized spatial correlation:

$$r(\mathbf{p}, \mathbf{q}) = J_0\left(\frac{2\pi\|\mathbf{p} - \mathbf{q}\|_2}{\lambda}\right), \quad (72)$$

⁸large w.r.t. the wavelength.

⁹Although this spatial correlation model fits many scenarios, it is by no means a universal model for the shadowing process, see [81]

where $J_0()$ is the Bessel function of first kind and zeroth order. It is possible to simulate the 2D random field representing the small-scale fading with the Jakes model using numerical techniques such as those of [86]. If the conditions of the environment differ from those required in the Jakes model, (72) would not be a good model for the spatial correlation function. Alternative models have been developed in the literature see [83], but as with the jakes model, the decorrelation distance is generally around $\lambda/2$.

3) *Data driven Models*: Another approach consists of using machine learning techniques to *learn* the communications channel. For instance, in [87], in the context of an iterative CaTP problem, the authors use Gaussian processes to construct a radio map of the wireless channel. This radio map is iteratively updated with channel measurements. In [88], the authors predict the Received Signal Strength (RSS) of the link between a UAV and a BS using the ensemble method technique, which combines various machine learning models. In [89], the authors propose a machine learning technique to learn the channel map of a defined region using segmentation. The six-dimensional space of the transmitter and receiver positions is segmented into K partitions and a different stochastic model assigned to each partition. To do this, a clustering algorithm is run on the channel measurements data set in order to determine the K partitions. Then, the parameters of each stochastic model are trained with the measurements of the corresponding partition.

In [90], the authors developed a machine learning technique that uses satellite images, determines the position of trees, and then uses an artificial neural network to determine the channel loss depending on the transceivers' position. Some other works also use artificial neural networks to predict the channel loss [91]. The radio maps constructed using machine learning techniques can be highly accurate in the regions where the measurements have been taken, but obtaining such measurements can be costly and time consuming. In addition, these are often numerical maps without analytical expressions, thus making them unsuitable for mathematical analysis that could provide useful insight into how to solve CaTP problems. In the rest of this section, we will focus on analytical channel models. The reader interested in machine learning techniques for channel modelling can find more information in [92].

B. UAV Channel Models

The channel models described in the previous section were originally developed for mobile communications considering ground users and are well suited to ground MRs applications. In general, they are not appropriate for UAVs applications mainly because of the changing altitude of the UAV. Further, given the increasing attention being paid to the integration of UAVs in 5G networks [18], [19], for the sake of completeness of this tutorial, we next discuss briefly the modeling of UAV wireless channels, which is currently an active research topic [93], [94].

Before presenting the UAV channel models, let us discuss some particularities of UAV communications. For small-sized

UAVs, the receiver is close to the UAV's power electronics and to the motors which run continuously. As a consequence, sometimes the UAV's motors generate electromagnetic noise that interferes with the UAV's own receiver [95].

Another phenomenon is airframe shadowing [93]. This occurs when the frame of the UAV itself partially blocks the LoS. Consider a multirotor UAV with an antenna on its top surface (i.e., the UAV's surface facing the sky) that is communicating with a ground station. Assume that the UAV moves away from the ground node. To do this, the multirotor UAV has to tilt in such a way that its bottom surface (i.e., the UAV's surface facing the ground) is slightly orientated towards the ground node. This can fully or partially block the LoS between the ground station's antenna and the UAV's antenna. In the case of fixed-wing UAVs, airframe shadowing can occur when the UAVs turn. In turning, they usually change their roll by controlling their ailerons. During this manoeuvre, one wing tilts up and the other tilts down. This tilting of the wings might temporally block the LoS with other communication nodes. The severity of the airframe shadowing, for both types of UAVs, depends on the airframe or wings material, its size, its shape, antenna location on the UAV's frame, and UAV trajectories. This phenomenon has been observed in practice, but, as mentioned in [93], [94], has not yet been fully studied.

The communications channel gain depends on the relative orientation of the transmitting and receiving antennas. During the flying phase, a multirotor UAV must tilt, thus changing its antenna orientation. As a consequence, the communication channel observed when a multirotor UAV hovers is different than when they move [96]. Similarly, during turning manoeuvres, a fixed-wing UAV has to tilt, thus changing its antenna orientation. The communications channel observed when fixed-wing UAVs move on a straight line is different than when they are turning. We also note that the location and orientation of the antenna on the UAV has a significant impact on the communications channel, as shown experimentally in [97], [98], [99], [100].

The UAV channel models can be divided into two types. The first consists of air-to-ground channels, which characterize the channels between a UAV and ground users or ground BS. The second consists of air-to-air channels, which characterize the channels between flying UAVs.

1) *Air-to-ground channels*: The air-to-ground channel communication models the link between a UAV and a ground user, such as a control station or a 5G BS. The properties of this channel depend not only on the distance between both nodes, but also on the UAV altitude and on the **elevation angle**¹⁰. As the elevation angle increases, the probability of LoS between both nodes also increases; LoS links present lower losses than non-LoS links. As the UAV altitude increases, the elevation angle increases along with the distance between the nodes. For instance, one illustrative model that describes such effects is [101]:

$$\begin{aligned} \mathcal{H}(\mathbf{p}(t), \mathbf{q}(t)) [dB] &= -20 \log (4\pi\lambda \|\mathbf{p}(t) - \mathbf{q}(t)\|_2) \\ &+ \xi(\mathbf{p}(t), \mathbf{q}(t)), \end{aligned} \quad (73)$$

¹⁰The angle of vector $\mathbf{p}_{UAV} - \mathbf{p}_G$ measured w.r.t. the horizontal plane, where \mathbf{p}_{UAV} and \mathbf{p}_G is the position of the ground node.

where the first term represents the average path loss and $\xi(\mathbf{p}(t), \mathbf{q}(t))$ represents the shadowing. If there is line of sight, then $\xi(\mathbf{p}(t), \mathbf{q}(t)) \sim \mathcal{N}(\mu_{LOS}, \sigma_{LOS}^2)$. Otherwise, $\xi(\mathbf{p}(t), \mathbf{q}(t)) \sim \mathcal{N}(\mu_{NLOS}, \sigma_{NLOS}^2)$. To complete this channel model, we also have to consider the probability of having line of sight, which can be expressed as:

$$P_{LOS}(\mathbf{p}_{UAV}, \mathbf{q}) = \frac{1}{1 + a \exp\left(-b \left[\frac{180}{\pi} \sin^{-1}\left(\frac{z_{UAV}}{d_h}\right) - a\right]\right)}, \quad (74)$$

where z_{UAV} is the altitude of the UAV, d_h is the horizontal distance between \mathbf{p}_{UAV} and \mathbf{q} , and the coefficients a and b are environment dependent.

Note that the model (73)-(74) does not take into account small-scale fading. As mentioned in [94], small-scale fading in air-to-ground channels often follows a Ricean distribution whose properties depend on the UAV altitude and the surroundings of the ground node. There are also approaches which use 3D numerical maps of the region of operation to determine the channel model [102]. We refer the reader to the survey in [94] for more detailed information about the air-to-ground UAV communications channels.

2) *Air-to-air channels*: The modeling of ground-to-air channels is not yet well studied, but the situation in the case of air-to-air channels (communications channels between flying UAVs) is worse since there are fewer studies and measurement campaigns focusing on this type of channels [93]. When the altitude of two UAVs is low, the floor and other objects on the surface (e.g. hills, buildings, and trees) influence the channel. However, as the altitude of the UAVs increases, such influences weaken. As the altitude of both UAVs increases, the channel tends to consist of a LoS and tends to behave like the *free-space* channel described in section III-A1.

It has been observed experimentally that when the UAVs operate on in open field with a floor that is flat enough, the propagation channel follows a two-ray model [93]. As the altitude of the UAVs increases, the strength of the reflected path decreases. Further, when the UAVs are operating over bodies of water such as lakes, the strength of the reflected path is stronger than when operating over land.

The constructive and destructive interference between the LoS and reflected waves described by the two-ray model can statistically be described with the small-scale fading. This is the approach taken in [103] where they showed experimentally that the air-to-air channel model can be modelled as follows:

$$\mathcal{H}(\mathbf{p}(t), \mathbf{q}(t), t) = \frac{h(\mathbf{p}(t), \mathbf{q}(t), t)}{L_P(\mathbf{p}(t), \mathbf{q}(t))}, \quad (75)$$

where the pathloss term $L_P(\mathbf{p}(t), \mathbf{q}(t))$ follows the *free space* model and the small-scale fading term is well described by a Rician distribution with height dependent parameters:

$$p_h(x) = \frac{x}{\sigma_0^2} \exp\left(\frac{-x^2 - \rho^2}{2\sigma_0^2}\right) I_0\left(\frac{x\rho}{2\sigma_0^2}\right), \quad (76)$$

$$\sigma = ah^b + c, \quad (77)$$

where $x \geq 0$; ρ and σ are the strength of the dominant and scattered components; h is the altitude of the UAVs (both UAVs are assumed to have the same altitude); with $a, b < 0$

and c being parameters to be fitted numerically according to the environment. Finally, we refer the reader to the survey in [93] for more detailed information about the air-to-air UAV communication channels.

C. Performance metrics

In CaTP, the communication aspects are taken into consideration in the optimization problem either in the target function or in the constraints. This requires the use of metrics to quantify the performance of wireless communication. Next, we discuss the metrics that are most relevant for CaTP.

- 1) **Channel quality**: one way in which the channel quality can be assessed is by measuring its power, using the Channel-to-noise Ratio (CNR) and the Signal-to-noise Ratio (SNR). The instantaneous CNR [5] at the receiver can be expressed as:

$$\text{CNR}(\mathbf{p}(t), \mathbf{q}(t), t) = \frac{|\mathcal{H}(\mathbf{p}(t), \mathbf{q}(t), t)|^2}{\sigma^2}, \quad (78)$$

where $\mathbf{p}(t)$ and $\mathbf{q}(t)$ are the positions of the transmitter and the receiver, and σ^2 is the power of the thermal noise generated at the receiver. The mean CNR is $\mathbb{E}[\text{CNR}(\mathbf{p}(t), \mathbf{q}(t), t)]$ where the expected value is taken w.r.t. the small-scale fading and the shadowing. The SNR is the CNR multiplied by the transmission power, which can be time-variant.

Another important metric is the Received Signal Strength (RSS) [104]. It measures the power of the received signal and the reason behind its importance is that many receivers in the market provide the Received Signal Strength Index (RSSI) (a discretized version of the RSS). In practice, many algorithms resort to working with the RSSI. Note that the SNR can be estimated from the RSSI if the noise power has been previously estimated. Finally, the SNR and the RSS are proportional to the CNR only if the transmitted power is constant, see section III-D.

- 2) **Error rate**: in some cases, one can be more interested in the performance of the communication system, rather than in the channel quality. The principal way of evaluating the performance of a communication system is by quantifying the errors that occurred in the transmission. This is done by calculating the Bit Error Rate (BER) or by the Packet Reception Ratio (PRR) [105], which measure how many packets were successfully received without errors. These metrics evaluate the performance of the communication system, and thus strongly depend on the specifications of the system, including the modulation scheme, and the communication protocols.
- 3) **Channel capacity**: the channel capacity was first introduced by Claude Shannon in 1948 in [106]. It is an upper bound on the maximum bit rate, given channel conditions, for which an arbitrarily low BER can be reached. Its mathematical expression depends on the information that the transmitter and the receiver have about the channel as well as on the power transmission strategy. When the channel is estimated at the receiver

and the transmitter uses constant transmission power, then the channel capacity is given by [107]:

$$C = B \int_0^\infty \log(1 + \gamma) p(\gamma) d\gamma, \quad (79)$$

where γ is the SNR, and $p(\gamma)$ its p.d.f.; and B is the bandwidth of the transmitted signal.

D. Energy consumption

Although often the MR's energy consumption is mostly due to motion, this is not always the case, as shown in the experiments presented in [50]. The μ controller, the CPU as well as the sensing systems can consume an amount of energy which may be comparable to the amount of energy spent in motion. The same applies to the MR's communication system. The energy consumed by the communication system is mainly determined by the transmission power. Next, we discuss transmission strategies.

- 1) **Constant power transmission:** all signals are transmitted with constant average power. As a consequence, the transmitter's energy consumption depends on the transmission time, but is independent of the transmitter and receiver positions. In this scenario, the SNR depends on the positions of the transmitter and the receiver through the spatial variations of the channel.
- 2) **Adaptive power transmission:** the transmitter adapts its power to ensure a certain power P_{ref} for the received signal. The power is adapted as follows:

$$P = \frac{P_{ref}}{|\mathcal{H}(\mathbf{p}(t), \mathbf{q}(t), t)|^2}, \quad (80)$$

P_{ref} is selected to ensure a certain quality of service. The transmission power in (80) can take any arbitrarily large value. In practice, the transmission power is limited to a certain value P_{max} by the hardware limitations or by legal regulations. If the intended transmission power is smaller than P_{max} , then the actual transmission power is (80). On the other hand, if the intended transmission power is larger than P_{max} (usually due to a poor channel gain), then it is not possible to satisfy the desired power P_{ref} at the receiver; the most common action in this scenario is to refrain from transmitting and say that an outage has occurred. Thus, the transmission power can be written as:

$$P = \begin{cases} \frac{P_{ref}}{|\mathcal{H}(\mathbf{p}(t), \mathbf{q}(t), t)|^2} & \text{for } \frac{P_{ref}}{|\mathcal{H}(\mathbf{p}(t), \mathbf{q}(t), t)|^2} \leq P_{max}, \\ 0 & \text{otherwise,} \end{cases} \quad (81)$$

A common practice for mathematical simplicity and tractability is to assume $P_{max} \rightarrow \infty$ (i.e., disregard the power limitation).

Finally, the energy consumption at the receiver is generally considered constant. Usually it is significantly lower than that of the transmitter and is hence often neglected in the analysis.

E. Final comments on communications models

We have provided an overview of communication systems and basic channel models for both ground MRs and UAVs. We also discussed the special characteristics of UAV channel models. Another special scenario that can be important for some CaTP applications, such as rescue and search operations, is communication inside tunnels and underground mines. This type of channel models are outside the scope of this tutorial, and interested readers are referred to [108], [69], [109].

The models presented in this section are narrowband models, which are the most basic models. More complex and elaborate models include wideband communication channel models which take into consideration how the channel varies w.r.t. the frequency. Also, we must mention that when one of the transceivers moves quickly, Doppler shift occurs and affects the received signals. This phenomenon can be of particular importance when dealing with fixed-wing UAVs since they can fly at high speeds.

IV. COMMUNICATIONS-AWARE TRAJECTORY PLANNING

As mentioned in section I, Communications-aware Trajectory Planning (CaTP) is trajectory planning in the context of Communications-assisted Robotics (CaR) and Robotics-assisted Communications (RaC) applications. CaTP problems aim to design trajectories where both communications (e.g., communication energy consumption, quality of the communications link, number of transmitted bits) and robotics aspects (e.g., kinematic and dynamic constraints, motion energy consumption) are simultaneously considered. We begin with some preliminary concepts.

A particular case of CaTP is the Communications-aware Path Planning (CaPP) problem. The trajectory and path are defined as follows.

Definition 1 (Path). *The path followed by a robot from time instant t_1 to t_2 is defined as $\mathcal{P}(\mathbf{p}(t), t_1, t_2) \triangleq \{\mathbf{p}(t) | t \in [t_1, t_2]\}$, where $\mathbf{p}(t)$ is the position of the robot at time instant t .*

Definition 2 (Trajectory). *The trajectory followed by a robot from time instant t_1 to t_2 is the description of the robot's position at each instant $t \in [t_1, t_2]$ and can then be described as $\mathcal{T}(\mathbf{p}(t), t_1, t_2) = \{\mathbf{p}(t), t | t \in [t_1, t_2]\}$.*

The path consists of the collection of all the points visited by the MR without specifying when and without any velocity information. On the other hand, the trajectory gives not only information about the points visited by the MR, but also a temporal description of the change of the MR's position over time. The trajectory can also be considered as the combination of the path and the MR's velocity profile.

From the application point of view, a CaTP problem can be cast as either a CaR or a RaC task. We can also classify CaTP problems depending on what is being optimized into three categories. In the first category, the objective is to design the MR's full trajectory, i.e., path and velocity profile. In the second category, the translational velocity is given (e.g., constant speed) and the objective is to design the MR's path; this is a CaPP problem. In the third category, the path is given

and the objective is to design the translational speed profile with which the MR will follow the given path, see for example [105].

CaTP problems can also be divided according to the type of trajectories: **predetermined** trajectories and **adaptive** (also referred to as reactive) trajectories. Predetermined trajectories are designed before they are executed by the MR. Adaptive trajectories are created and modified as the robot executes them. Note that the MR could use a predetermined trajectory as an initial guide and then implement an adaptive mechanism to adapt the trajectory in real-time in response to new information obtained from the environment. In this tutorial, we focus on predetermined trajectories.

The optimization method and the optimum trajectory resulting from solving CaTP problems strongly depend on the information that is available about the wireless channel when solving the optimization problem. Some possible scenarios are described next.

- 1) **Estimate of full RF map is available:** in this scenario, we have full knowledge of the RF map (or a good estimate of it). In other words, we have knowledge (or an estimate) of $\mathcal{H}(\mathbf{p}, \mathbf{q}(t), t)$ in (61) for all $\mathbf{p} \in \mathcal{W}$ and all $t \in [0, T]$ where \mathcal{W} is the workspace where the MR can move and $\mathbf{q}(t)$ is the position of the other node. The knowledge of the RF map can be obtained by directly implementing ray tracing [71], [72], [73], using channel simulators [110] to predict the channel map in a specific region.
- 2) **Estimate of the path-loss+shadowing RF map is available:** In this case, we only have estimates of $s(\mathbf{p}(t), \mathbf{q}(t))$ and $L_P(\mathbf{p}(t), \mathbf{q}(t))$ in (68). This information can be obtained if, prior to the optimisation procedure, channel measurements are taken and then used to reconstruct the full map of the pathloss and shadowing [76].
- 3) **Full statistical knowledge is available:** here, we know the statistical distribution (p.d.f.) and the spatio-temporal correlations of the shadowing $s(\mathbf{p}(t), \mathbf{q}(t))$ and the small-scale fading $h(\mathbf{p}(t), \mathbf{q}(t), (t))$.
- 4) **Statistical distribution knowledge is available:** in this case, we know the p.d.f. of the shadowing and the small-scale fading, but ignore their spatial correlations.

Now that we have introduced some preliminary concepts for CaTP problems, we will discuss in the next subsection the mathematical structure of a generic CaTP optimization problem to obtain a predetermined trajectory.

A. General Structure

The general structure of a CaTP optimization problem which aims to determine a predetermined trajectory of a single MR can be described as:

$$\begin{aligned} & \min_{\mathbf{u}, \mathcal{C}, \mathcal{T}} J(\mathbf{u}, \mathcal{C}, \mathcal{T}) \\ & \text{s.t.} \\ & \text{motion model,} \\ & \text{channel model,} \\ & \text{trajectory constraints,} \\ & \text{communications constraints} \end{aligned} \quad (82)$$

where \mathbf{u} is the MR's control signal; \mathcal{C} is the set of all communication related parameters to be optimized, such as modulation order or transmission power¹¹; \mathcal{T} is the set of the remaining parameters to be optimized which are not directly related to the communication system, such as the completion duration of the trajectory.

This generic CaTP problem (82) is composed of five elements: the optimization target $J(\mathbf{u}, \mathcal{C}, \mathcal{T})$; a motion model for the MR describing how its *state* behaves according to the control signal \mathbf{u} ; a wireless channel model describing how the received and transmitted signals behave depending on the position and orientation of the MR; some trajectory related constraints; and finally, constraints related to the communication system performance and/or goals. We now discuss these five elements in more detail.

- 1) **Optimization target:** in CaTP problems, the optimisation target (a.k.a. cost function) can take different forms, but can be divided into three classes. The first class has communications and robotics terms, the second class has only robotics-related terms, and the third class has only communications-related terms. A common robotics-related term used in the cost function of CaTP problems is the energy consumed by the MR while tracking the desired trajectory. Another robotics-related term is the travelled distance travelled by the MR; this implicitly assumes that the energy consumption due to motion can be accurately obtained from the distance travelled by the MR. Another common robotics-related metric is the total time that the MR takes to complete the designed trajectory. Regarding the communications-related term in the optimization target, typical examples are the energy spent by the MR's communication system, the total number of bits transmitted, and the time during which the robot was disconnected from the communication network. In subsections IV-B and IV-C, we will discuss in further detail the form and properties that this optimization target can take in different problems. Further, in some problem formulations, the optimization target $J(\mathbf{u}, \mathcal{C}, \mathcal{T})$ can be replaced with a constant, in which case the optimization problem (82) becomes a constraint satisfaction problem and its solution would result in a trajectory (or set of trajectories) that satisfies all of the set constraints.
- 2) **Motion model:** this relates the state of the MR to the control signal \mathbf{u} . The motion model consists of kinematic or dynamic models like the ones discussed in section II. As mentioned in section II, many motion models are nonlinear with respect to the control signal \mathbf{u} , but they can also be linearized to simplify the control and the optimization procedure (although the solution would then become suboptimal).
- 3) **Channel model:** the selected channel model must take into account the physical environment where the MR and the other nodes communicating with it are located (e.g. indoor or outdoor, urban or rural scenario, etc.). It is also important to consider if the links involved are ground-

¹¹Note that if all of the communications parameters are fixed, then $\mathcal{C} = \emptyset$.

to-ground (the MR and the other node located at ground level), air-to-ground (i.e., a UAV and a ground node), or air-to-air (i.e., communication between two UAVs).

4) **Trajectory constraints:** these constraints directly restrain the shape of the trajectory and the time in which it is completed. A constraint of this category defines the workspace $\mathcal{W}(t)$ where the MR can operate, and thus the path must lie within. The workspace is determined by taking into account obstacles (e.g. trees and/or walls) and regulations (e.g. regulations regarding the maximum flying altitude of UAVs).

Trajectory constraints can ensure a certain trajectory smoothness so that the MR is able to track it. The simplest way to achieve this is by ensuring that the MR's trajectory is n -times derivable over the full temporal support considered for the trajectory. Another way to control the smoothness of the trajectory is by introducing the following set of constraints:

$$\left| \frac{d^n x_k(t)}{dt^n} \right| \leq v_{j,k}, k = 1, 2, \dots, K, n = 1, 2, \dots, N, \\ t \in [0, T] \quad (83)$$

where $x_k(t)$ is the k th entry of the K -dimensional state vector describing the motion of the MR. We can also introduce constraints on the curvature of the path so that the MR does not have to perform abrupt turns that could violate its kinematic constraints. We must highlight that if the motion model selected to describe the motion of the MR is oversimplified, then introducing this type of constraints to control the smoothness of the trajectory and the curvature of the path can ensure that the resulting optimum trajectory does not violate the dynamic and kinematic constraints of the physical MR.

We can also constrain the initial and final states of the MR according to one of the following type of trajectories: **open trajectories** and **closed trajectories**. Open trajectories start and end in different points within the workspace \mathcal{W} , while closed trajectories start and end in the same exact point. Closed trajectories are sometimes selected for repetitive tasks, such as data transport [7] or surveying tasks. In order to ensure a closed trajectory, we must satisfy:

$$\mathbf{x}(0) = \mathbf{x}(T) = \mathbf{x}_0. \quad (84)$$

Another type of constraints acts directly on the control signal \mathbf{u} , thus limiting for example the velocity and/or acceleration of the robot. One instance of this constraint may be:

$$\|\mathbf{u}\|_\infty \leq V, \quad (85)$$

which models the saturation of the physical actuators used to control the MR. When the entries of the control signal vector \mathbf{u} represent the voltage inputs to each of the MR's motor, the constraint (85) individually limits the voltage applied to each motor.

5) **Communications constraints:** these act on the overall communication system performance or directly on the wireless channel experienced by the MR along the

whole trajectory. When stochastic channel models are used, the constraints related to the wireless channel are probabilistic. For example, we can constraint the MR to transmit along its trajectory an average of N bits or higher:

$$\int_0^T \mathbb{E}[R(\text{SNR}(\mathbf{p}(t), \mathbf{q}(t), t))] dt \geq N \quad (86)$$

where $\text{SNR}(\mathbf{p}(t), \mathbf{q}(t), t)$ is the instantaneous SNR observed at time instant t over the link between the MR located at $\mathbf{p}(t)$ and the other node located at $\mathbf{q}(t)$. The function $R(\cdot)$ determines the bit rate transmission as a function of the instantaneous SNR. This function $R(\cdot)$ depends on the modulation scheme. The expected value in (86) is taken w.r.t. all possible wireless channel realizations. To introduce this constraint, the designer needs to know the first order statistics of the wireless channel model. Because of the stochastic nature of the wireless channel, the constraint (86) does not ensure that the MR will be able to always transmit at least N bits, but rather that robots following the same trajectory in the same environment will transmit at least N bits on average. Note that (86) assumes that the transmission process is continuous (we observe this from the integral and the fact that the integrand is treated as a continuous function of time). Even if the transmission is not a continuous process (the data is transmitted in packets and not in a continuous and uninterrupted flow), we can for simplicity assume that it is a continuous process since the dynamics of the motion process is, in general, much slower than the dynamics of the transmission process.

There are also constraints acting directly on the wireless channel. The advantage of directly constraining the wireless channel resides in the fact that it makes the optimisation problem independent of the used communication system (e.g. modulation type). One common constraint of this type has the following form:

$$\Pr(\text{SNR}(\mathbf{p}(t), \mathbf{q}(t), t) \geq \gamma_0) \geq 1 - \epsilon, \quad \forall t \in [0, T]. \quad (87)$$

This constraint ensures that during the whole trajectory, the MR's communication system experiences an SNR larger than γ_0 with a probability of $1 - \epsilon$. If the minimum SNR for the MR to establish communication is γ_0 , then by satisfying the constraint (87), we ensure that the MR stays connected during the whole trajectory with a probability of $1 - \epsilon$.

Not all the five elements in (82) are essential in all CaTP optimisation problems. Only the MR motion model (sometimes not explicitly mentioned when it is too simple), the channel model, and the optimisation target are essential. Regarding the constraints, there are four different possibilities:

- 1) Case 1: the optimisation target considers both communications and robotics aspects; in this case, we might require neither trajectory nor communications constraints.
- 2) Case 2: the optimisation target considers only robotics aspects. For example, the optimisation targets consider

only the motion energy of the MR (the communication energy is assumed negligible against the motion energy). In this case, the CaTP problem includes communications constraints, and has a reduced set of trajectory constraints, e.g. only the initial and final positions of the MR.

3) Case 3: the optimization target considers only the communications aspects. Here, the CaTP may have no communication-related constraints.

The constraints discussed above are **hard constraints**, i.e., either they are satisfied or they are not. In some cases, this type of constraints can cause issues in the optimization problem. One of these issues is related to the unfeasibility of the optimization problem (82). In some cases, there might be certain parameters' values that make it impossible to satisfy some hard constraints of the CaTP problem, rendering it unfeasible. In complex CaTP problems with many parameters and complicated constraints, it might be hard to identify this situation. Another issue is related to the performance of the solution to the optimization problem (82). It might happen that one trajectory slightly violates a hard constraint in (82), achieving a significantly lower value in the optimization target than the actual optimum trajectory that satisfies all the constraints. These issues can be solved by relaxing some hard constraints and transforming them into *soft constraints*.

Let us consider a general inequality constraint, $g(\mathbf{u}, \mathcal{C}, \mathcal{T}) \leq 0$. There are two techniques to relax this hard constraint. The procedures to relax equality constraints are similar to those used for inequality constraints and require minor modifications.

The first technique consists of transforming the hard constraint into a penalization term added to the optimization target in (82). This penalization term can for example be expressed as:

$$\mathcal{P}_f = \mu_1 \exp(\mu_2 g(\mathbf{u}, \mathcal{C}, \mathcal{T})) \quad (88)$$

where $\mu_1, \mu_2 > 0$ are large real constants. The term (88) adds a large penalty to the optimization target when the constraint $g(\mathbf{u}, \mathcal{C}, \mathcal{T}) \leq 0$ is violated, i.e., when $g(\mathbf{u}, \mathcal{C}, \mathcal{T}) > 0$. If $g(\mathbf{u}, \mathcal{C}, \mathcal{T}) \leq 0$ is satisfied, $\mathcal{P}_f \approx 0$. We have used this technique in [4] to avoid obstacles in a CaTP problem.

The second technique consists of the utilization of slack variables [111]. To relax the inequality constraint mentioned above, this technique consists of changing the constraint to $g(\mathbf{u}, \mathcal{C}, \mathcal{T}) \leq s_g$ with $s_g \geq 0$, and adding to the optimization target in (88) the term $k_s s_g^2$ with $k_s \geq 0$. The slack variable s_g allows $g(\mathbf{u}, \mathcal{C}, \mathcal{T}) \leq 0$ to be slightly violated. The degree of this violation is modulated with the parameter k_s . Note that when $k_s = 0$, the constraint becomes a hard one.

Some hard constraints in (88) are related to the desired performance and are generally imposed by the designer. For instance, constraints of this type can act on the time to complete the mission, the final position of the robot, or the minimum number of bits to transmit. This type of constraints can be relaxed if the particular application, for which the CaTP problem is solved, tolerates the relaxation. On the other hand, there are hard constraints that are imposed by the physical world. Such constraints include the dynamics of the MR, its

kinematic model, the presence of obstacles, or the maximum transmission power. The relaxation of this type of constraint might result in solutions that will not work on the real world.

Now that we have described the structure of a generic CaTP problem, we will next discuss in more details different types of CaTP problems, which we classify into loose categories.

B. Minimum Energy Trajectories

The **Minimum Energy Trajectory with Communications Objectives** problem is one of the most illustrative CaTP problems. It considers a MR that accomplish a certain task involving both motion and communications. The objective is to design the MR's trajectory so as to perform the desired task while minimizing the overall energy consumption (i.e., communications energy plus motion energy). This is important since MRs usually draw their energy from an on board battery which feeds not only their locomotion system, but their communications system as well. By minimizing the overall energy consumption, we may either reduce the MR's battery size (and thus its cost) or increase the MR's operational time, allowing it to fulfil more and longer tasks. Note that this problem may be irrelevant for tethered MRs since they receive energy from an external source [112].

At first glance, we could say that the energy spent by the MR in communications is negligible compared to the energy spent in motion, but as mentioned in section III-D, this is not always true. As shown in [113], the energy consumed by the communication system may be comparable to the energy spent in motion. This depends on various aspects, such as the amount of data transmitted, the distance to the node communicating with the MR, and the adopted power transmission strategy. In addition, as mentioned in [23], the size of the MR also determines how significant the communication power consumption is against the motion power consumption. For a small MR, the power spent in communications can be significant w.r.t. the power consumed in motion; however, for larger and heavier robots, the communication power might be negligible w.r.t. the power consumed in motion.

Mathematically, the Minimum Energy Trajectory with Communications Objectives problem is stated as an optimization problem with the following optimization target:

$$J = E_{\text{motion}}(\mathbf{u}, 0, T) + E_{\text{comm}}(\mathbf{u}, 0, T), \quad (89)$$

where $E_{\text{motion}}(\mathbf{u}, 0, T)$ and $E_{\text{comm}}(\mathbf{u}, 0, T)$ are the energies spent by the MR in motion and in communications, respectively, from time instant 0 up to time T using the control signal \mathbf{u} ; T is the task completion time that can be either a fixed parameter or an optimization variable. We must mention that the power transmission policy selected (see section III-D) drastically affects the optimum trajectory and the complexity of the problem.

If a constant transmission power strategy is selected for the MR and a continuous transmission is considered, then communication energy consumption becomes:

$$E_{\text{comm}}(\mathbf{u}, 0, T) = PT. \quad (90)$$

If the task completion time T and the constant transmission power P are fixed, then the communication energy becomes

a constant term in the cost function (89) and the problem becomes that of a minimum motion energy trajectory design, subject to communications constraints, which are often related to the quality of the received signal. Since the transmission power is constant, the received power will depend on the channel gain, which depends on the actual MR's trajectory itself.

On the other hand, if a transmission power control mechanism is used by the MR (see section III-D), then the communication energy consumption in (89) depends on the particular trajectory followed by the MR. If the transmission power is given by (80), the received power is always P_{ref} , and thus the quality of the signal received is independent of the trajectory. However, (80) assumes no bound on the maximum transmission power. If we consider maximum transmission power, then the actual transmission power consumption is given by (81). Additional constraints are needed to ensure that the robot can communicate. We illustrate this with the following example: an MR must depart from a point A and arrive at a point B while communicating with a base station using the power control strategy (81). We want to optimize its trajectory so that total energy (89) is minimized. If the channel observed along the minimum motion energy path between points A and B is so poor that no transmission is possible along this path (i.e., $E_{comm}(\mathbf{u}, 0, T) = 0$), this would be the optimum path for our problem but the issue is that no communication would occur. Therefore when using the transmission power policy in (81), we must also include constraints to ensure that communication requirements are satisfied.

We can find one instance of this problem in [48] where the authors consider the problem of a ground MR that needs to communicate with a base station and must reach a predefined target point. The path is optimized so that the total energy consumption is minimized while completing the entire task. In [5], the authors consider the problem of minimizing the total energy consumption of a ground MR that must reach a target point in a predefined time and transmit a certain amount of data to a base station. In [114], [115], we consider the problem of a ground MR that must communicate with a BS through a communication channel experiencing small-scale fading. We design the trajectory so that the MR can find a good location for transmission. We optimize this trajectory so that the total energy (i.e., communications and motion energies) is minimized.

C. Energy Efficient Trajectories

In the previous subsection, we discussed the Minimum Energy Trajectory with Communications Objectives problem. We now discuss a more general CaTP optimization problem where the communications aspect considered in the optimization target is different from the communication energy consumption. This type of problem can be applied to an MR whose motion power consumption is significantly larger than the communication power consumption. In this scenario, the objective is usually to use as little energy in motion as

possible to complete a communication related task, which depends on the performance of the communication system and/or the channel quality. In other words, the objective is to complete a task in an energy efficient manner. We refer to this type of trajectories as Energy Efficient Communications aware trajectories.

One way to achieve this is to use the following optimization target:

$$J = \theta E_{motion}(\mathbf{u}, 0, T) + (1 - \theta) f_{comm}(\mathbf{u}, 0, T) \quad (91)$$

where $E_{motion}(\mathbf{u}, 0, T)$ is the motion energy consumed by the MR, $f_{comm}(\mathbf{u}, 0, T)$ is a communication metric to be minimized, and $\theta \in [0, 1]$ is a design parameter that determines the importance of one objective with respect to the other. Since both terms have generally different physical units, we need to normalize them to ensure that they vary, more or less, in the same numerical range. This is highly convenient for avoiding problems when solving the CaTP optimization problem numerically. Another way of formulating an energy efficient communications-aware trajectories problem is by maximizing the following objective function:

$$J = \frac{g_{comm}(\mathbf{u}, 0, T)}{E_{motion}(\mathbf{u}, 0, T)} \quad (92)$$

where $g_{comm}(\mathbf{u}, 0, T)$ is a communications metric, to be maximized. Here, (92) maximizes the ratio of two metrics. The advantage of doing this is that we can easily combine metrics having different units and do not need to normalize them, nor to select an adequate weight parameter. Nevertheless, the fact that there is no weight parameter, this optimization target lacks flexibility by being able to produce only a single trajectory, rather than a whole Pareto front of possible trajectories.

Yet another way to tackle energy efficient communications-aware trajectories is to select the optimization target as the motion energy and then introduce the communications objective as constraints. By doing this, the MR will reach the communications objective using the minimum motion energy possible. The complementary form is also possible, where the cost function is a communications metric and constraints are imposed on the motion energy. In this approach, the MR expends a certain amount of energy as efficiently as possible to optimize the communications metric.

For instance, in [84], the authors considered the problem of a MR that must sense some area while maintaining communication with a base station. The objective is to design a trajectory to complete this task while maintaining appropriate channel quality throughout the entire trajectory. In [116], the authors considered the problem of a MR that must find a position in which the channel gain is high enough to allow for communication with a certain quality of service, while using the minimum motion energy possible. In [117], the authors considered a problem in which a team of MRs all have a copy of the same message and need to transmit the message to a base station, which combines the signals received from all the MRs. The objective is to maximize the total received signal power. To achieve this, the MRs need to find positions where the channel gain is high enough using as little energy as possible. In [118], the authors considered the

problem of designing the path for an energy-limited UAV that must reach a certain target point. During the whole trajectory, it must also satisfy certain channel constraints in order to transmit video while moving. In [119], the authors highlight the importance of considering the wireless communication links for UAVs when designing paths; they considered the notion of communication coverage of a UAV's path. In [120], [121], we considered the problem of a MR that must reach a certain target point and transmit data to a base station; the trajectory is optimized so as to spend as little energy in motion as possible, while transmitting as much data as possible. The objective function in [120], [121] takes the form of (91) where the communication-related term represents the number of bits transmitted by the MR. In [4], we extended this by considering a general communications term that could represent various types of communications-related criteria.

D. Other Trajectory Design Strategies

In the previous subsections, we discussed with some detail minimum energy CaTP and energy efficient CaTP problems. For completeness, we will next briefly discuss some other types of CaTP problems that represent interesting and exciting research opportunities. Some additional examples of problems related to CaTP can be found in [122].

- 1) **Trajectory design for Robotic relays.** A robotic relay is a MR that relays data between communicating nodes. They can be used to establish communication between two nodes, A and B (which may be either static or mobile), which cannot communicate directly as the channel between them is too weak. This can happen if both nodes are too far away from each other or if there are various obstacles between them. In this case, one or more robotic relays can be used to establish communication between nodes A and B . The advantage of using MRs as mobile relays instead of static relays is that they can adapt their positions to maintain or improve the performance of the system, regardless of any change in the environment or in the positions of the nodes A and B . This type of problem might be of particular interest to researchers working in swarm robotics.

In this problem, the objective is to optimize the trajectory of one or more MRs acting as robotic relays in order to have good end-to-end communication performance. For instance, in [123], the authors considered the scenario in which a chain of robotic relays must ensure communication between a static robot and a robot that is exploring a certain area. In [124], the authors addressed the problem of designing trajectories for robotic routers to ensure communication within an indoor environment. In [125], the authors considered the problem of a fixed-wing UAV relay for helping a terrestrial robot. In [126], the authors too considered a fixed-wing UAV relay between ground nodes and optimized its trajectory to maximize the end-to-end throughput. In [127], the authors developed an experimental platform for robotic relays. In [128], we considered the problem of optimizing the position of a robotic relay to transfer data from various sensors to a fusion center.

- 2) **Trajectory Design for Data Ferries.** Robotic data ferries operate similarly to robotic relays, except that they move between the nodes in order to physically transport data. Data ferries are suitable only in scenarios where the application using data to be transferred tolerate the delay introduced by the movement of the data ferry. In some cases, the source node produces data continuously, which requires to design a periodic (or quasi-periodic) trajectory. These periodic trajectories are optimized generally by maximizing the end-to-end throughput or maximizing the energy efficiency of the data transfer process (i.e., minimizing the energy cost of transferring one bit of data).

In [87], the authors considered the problem of designing a closed trajectory for a UAV acting as a data ferry between two nodes. The objective was to maximize the end-to-end throughput. In [129], we studied the problem of a ground MR acting as a ferry that must gather data from various sensors and then move towards a fusion center to deliver the data. We studied the tradeoff between the energy consumption of the MR and the end-to-end throughput. In [7], we considered the problem of a UAV acting as a data ferry between two nodes. We optimized its closed trajectory to maximize the end-to-end throughput. To do this, we parametrized the trajectory using Fourier series and then optimized the coefficients.

In [12], the authors optimize the trajectory of a UAV that collects the data from sensor nodes in an energy efficient manner for the network. In [130], we optimized a 3D closed trajectory for a quadrotor UAV to collect data in an energy efficient manner from various sensor nodes. What is interesting in this scenario is how as the UAV increases its altitude, the region that it covers grows, but the channel losses also grow. Thus, a careful optimization of the UAV altitude must be performed.

- 3) **Communications-aware Trajectory for PV equipped robots.** Recently, there has been an interest in adding solar PV panels to UAVs. One of the main motivations for adding PV panels to the UAVs is to extend their flying time as much as possible. This addition converts the UAVs into agents that can perform three main actions: transmit data, move, and recharge batteries through their solar panels. Interestingly, both the solar power production of the UAV's PV panels and the quality of its communications are a function of the UAV position. By giving the UAV the ability to produce energy, the CaTP problem becomes more complex. Indeed, we now have to consider not only the motion and communications aspects, but the energy generation aspect as well.

In [131], the authors consider the problem of optimizing the 3D trajectory of a UAV equipped with a PV solar panel that must provide a wireless communication service to ground users. The trajectory is optimized to maximize the overall throughput provided to the users during a certain amount of time. The trajectory is optimized while simultaneously taking into account

the communications, the solar power production, and the motion-induced energy consumption. In [132], the authors addressed the same problem; the UAV can produce energy for self-consumption, but can also sell it. In addition, the users are charged by the amount of data processed by the UAV. The objective is to optimize the UAV trajectory to maximize the overall revenue. In this problem, the energy and data transmitted are both translated into money, and thus the optimization target representing the revenue is a weighted sum of the data received by the UAV from the users, the energy consumed, and the energy sold. Note that this particular problem is a mixture of a CATP problem and a smart-grid problem. The authors in [133] consider a framework in which UAVs equipped with transceivers and PV panels forming part of a heterogeneous network must optimize their behaviour in order to minimize the overall energy consumption of the network, while providing certain service to the users.

4) **Trajectory Design for Small-Scale Fading Compensation.** As mentioned in section III-A, the small-scale fading provokes large variations in the channel gain over small distances (compared to the wavelength used). These variations can significantly degrade the performance of the communication system; thus, it is important to compensate this phenomenon. One way to perform this compensation is to control the position of the robot's antenna, which is done by controlling the position of the robot itself. By doing this, the robots can leverage the spatial variations of small-scale fading to improve in a smart fashion the channel gain observed. This problem can take two forms. In the first, the objective is to find a static position from which the robot will transmit its data. The robot explores a small region (compared to the wavelength) in order to find a suitable point for transmission. A trajectory planner is designed for such a task. In its second form, the robot must follow a certain path and can only control its linear velocity. In this case, a speed controller is designed to adequately compensate for the small scale fading. Broadly speaking, the general strategy that such controllers follow is to reduce the speed when the channel gain is high and increase the speed otherwise.

The authors in [105] considered a problem where a robot has to follow a predefined closed path and is able to stop at some points. A speed controller is designed so that the robot stops for a certain time at positions with high channel gain to communicate with a remote node. In [134], the authors experimentally show how by controlling the position of the robot, they can compensate for the small-scale fading. They designed short trajectories to perform this task. In [135], the authors also experimentally demonstrate this same principle by means of an antenna mounted on a turntable. In [136], we considered a ground MR harvesting RF energy and developed a trajectory planner that exploits small-scale fading to maximize the amount of energy harvested. The

path explored by the MR in this technique is restricted to a straight line whose length is optimized. In [137], we extended this trajectory planner by optimizing not only the length of the path, but also its shape. Furthermore, in [138], we developed a predetermined trajectory planner that allows a ground MR to find points with high channel gain in its vicinity in an energy efficient manner. In this technique, the MR explores a set of stopping points to determine the best position for communication. These stopping points are close to each other and the small-scale fading at those locations presents low spatial correlation. This ensures obtaining high channel gains while minimizing the amount of energy spent in motion for the exploration of the stopping points. We expanded upon this work in [21] by making the trajectory planner adaptive. The locations of the points are determined on the fly and in an iterative manner. At each time, the next point to be visited by the MR is calculated as a function of the channel measured in the current and previous points. Results show that this technique outperforms the technique presented in [138], but requires an estimate of the shadowing as well. We further investigated this technique in [139] by considering the problem in which a MR equipped with an antenna mounted on a rotary platform has to follow a predefined trajectory while communicating with a BS through a fading channel. We developed a feedback controller that continuously optimizes the position of the antenna and operates under time-varying fading. In [128], [129], we further extended this technique to optimize the position of a ground MR to compensate for the small-scale fading of multiple communication channels simultaneously.

5) **Communications-aware UAV Placement.** In the previously described problems, the main focus was on the robot's trajectory. In Communications-aware UAV placement problems, the focus is on the stopping (or final) positions of the UAV to provide a communication service to ground users, rather than on the full trajectory, although in some cases, the energy required by the UAV to reach a convenient final position was also of interest. For these problems, the wireless channel is modelled using 3D channel models, such as the ones presented in section III-A. In 5G, it is expected that drones will be part of the cellular networks to improve their performance. Therefore, this particular problem is of high interest. Note also that even if this is not a CATP problem, it requires similar tools and models. For this reason and its importance for future cellular networks, we will next briefly describe some instances of this problem.

For example in [140], the authors consider the problem of positioning UAVs for improving a cellular network. In [141], the authors optimize the altitude of a UAV to provide service to a cellular network. The authors of [142] address the problem of optimizing the 3D position of a UAV to maximize the number of covered users. In [143], the problem of optimizing the 3D position of

UAV to maximize the number of users covered by the network is considered, which maximizes the revenue of the network. In [144], optimization of the position of a UAV giving communications service to a user inside a vertical building is evaluated. The problem of a distributed algorithm is considered in [145] for the purpose of the iterative optimization of a position of a team of UAVs giving service to other users in a network.

6) **UAVs and physical security.** A recent and interesting application is the implementation of physical layer techniques [146] through the use of UAV to solve cybersecurity issues in cellular networks [147]. One interesting example of this type of problem is the joint optimization of the UAV's trajectory and communications strategy to improve the security of the network against eavesdroppers. The general strategy to achieve this is to use one or more UAVs to: (i) jam the eavesdropper to degrade its signal-to-noise ratio; (ii) act as relays between the BS and the targeted node so that the latter reduces its transmission power, thus decreasing the strength of the signals captured by eavesdroppers.

For example in [148], the authors consider the following problem. A source node A must transmit data to a destination node B via a UAV acting as a relay, but a malicious node E is acting as an eavesdropper. The problem addressed by the authors is the joint optimization of the UAV trajectory and the communications parameters (such as bandwidth and transmission power) in order to maximize the secrecy rate. The general strategy consists of degrading the communications channel between the UAV and the eavesdropper while improving the quality of the end-to-end communication between nodes A and B . The same authors addressed a more elaborate version of this problem in [149], [147]. In [150], the authors optimize the trajectory and communication parameters of a UAV that operates exclusively as a jammer. The setup consists of a source node S , a destination node D , an eavesdropper E , and a UAV jammer. The authors optimize the trajectory of the UAV jammer and its power in order to significantly degrade the the strength of the signal received by the eavesdropper while simultaneously minimising the impact on the node S . The reader may find more information about the optimization of the UAV trajectory to improve the cybersecurity of cellular networks in [151], [152], [153].

V. DISCUSSION AND CONCLUDING THOUGHTS

The growing interest for merging ground MRs and UAVs with communication systems is gaining momentum in both industry and academia. One of the main reasons for this is the surge of 5G technologies which aim to integrate UAVs into the cellular networks. Another important reason is the growing popularity of multi-robot systems where the MRs have to maintain communication links. In these applications, the communications and robotics aspects are closely interrelated. We discussed in section I some of the consequences of addressing these problems without an interdisciplinary approach.

An interdisciplinary approach is fundamental to fully exploit the maximum potential of this research area due to the strong entanglement between the robotics and communications aspects. In the hope of contributing to the quantity of material and quality of this research area, this tutorial provides the basic theory behind this still underdeveloped, yet promising research area. We have described different motion models for various types of ground and aerial MRs, as well as various channel models for different scenarios relevant to the CaTP problems. Additionally, we have provided a general mathematical formulation for CaTP problems for predetermined trajectories. Different ways have been shown in which the robotic motion models and the communications channel models can interact with each other within the formulation of CaTP problems. Finally, we have provided a brief application-oriented classification of different CaTP problems and other related problems.

PLACE
PHOTO
HERE

Daniel Bonilla Licea received his M.Sc. degree in 2011 from the Centro de Investigación y Estudios Avanzados (CINVESTAV), Mexico City. From May 2011 until June 2012, he worked as an intern in the signal processing team of Intel Labs in Guadalajara, Mexico. He received his PhD degree in 2016 from the University of Leeds, U.K. In 2016 he was invited for a short research visit at the Centre de Recherche en Automatique de Nancy (CRAN), France. In 2017 he collaborated in a research project with the Centro de Investigación en Computación (CIC) in Mexico.

From 2017 to 2020 he held a postdoctoral position at the International University of Rabat, Morocco. Currently he holds a postdoctoral position at the Czech Technical University in Prague, Czech Republic. His research interests are signal processing, and communications-aware robotics.

PLACE
PHOTO
HERE

Dr Ghogho (F'18) has received the M.Sc. degree in 1993 and the PhD degree in 1997 from the National Polytechnic Institute of Toulouse, France. He was an EPSRC Research Fellow with the University of Strathclyde (Scotland), from Sept 1997 to Nov 2001. In Dec 2001, he joined the school of Electronic and Electrical Engineering at the University of Leeds (England), where he was promoted to full Professor in 2008. While still affiliated with the University of Leeds, in 2010 he joined the International University of Rabat (Morocco) where he is currently Dean of

Doctoral College and Director of TICLab (ICT Research Laboratory). He is also a co-founder and co-director of the CNRS-Associated International Research Lab DataNet. He was awarded the UK Royal Academy of Engineering Research Fellowship in 2000 and the IBM Faculty Award in 2013. He was elevated to the grade of IEEE Fellow in 2018. His research interests are in signal processing, machine learning and wireless communication. In the past, he served as an associate editor of the Signal Processing Magazine, the IEEE Transactions on Signal Processing, the IEEE Signal Processing Letters, and the Elsevier Digital Signal Processing journal, and a member of the IEEE Signal Processing Society SPCOM Technical Committee, the IEEE Signal Processing Society SPTM Technical Committee, and the IEEE Signal Processing Society SAM Technical Committee. He is currently a member of the steering committee of the IEEE Transactions of Signal and Information Processing over Networks. He held invited scientist/professor positions at Telecom Paris-Tech (France), NII (Japan), BUPT (China), University Carlos 3rd of Madrid (Spain), ENSICA (Toulouse), Darmstadt Technical University (Germany), and Minnesota University (USA).

PLACE
PHOTO
HERE

Martin Saska received his MSc. degree at Czech Technical University in Prague, 2005, and his Ph.D. degree at University of Wuerzburg, Germany, within the PhD program of Elite Network of Bavaria, 2009. Since 2009, he is a research fellow at Czech Technical University in Prague, where he founded and heads the Multi-robot Systems lab (<http://mrs.felk.cvut.cz/>) and co-founded Center for Robotics and Autonomous Systems with more than 70 researchers cooperating in robotics (<https://robotics.fel.cvut.cz/cras/>). He was a visiting

scholar at University of Illinois at Urbana-Champaign, USA in 2008, and at University of Pennsylvania, USA in 2012, 2014 and 2016, where he worked with Vijay Kumar's group within GRASP lab. He is an author or co-author of >150 publications in peer-reviewed conferences with multiple best paper awards and more >40 publications in impacted journals, including IJRR, AURO, JFR, ASC, EJC, with >4000 citations indexed by Scholar and H-index 35. His team won multiple robotic challenges in MBZIRC 2017, MBZIRC 2020 and DARPA SubT competitions (<http://mrs.felk.cvut.cz/projects/mbzirc>, <http://mrs.felk.cvut.cz/mbzirc2020>, <http://mrs.felk.cvut.cz/projects/darpa>).

REFERENCES

- [1] A. Gasparri, L. Sabattini, and G. Ulivi, "Bounded Control Law for Global Connectivity Maintenance in Cooperative Multirobot Systems," *IEEE Transactions on Robotics*, vol. 33, no. 3, pp. 700–717, 2017.
- [2] Y. Gao, H. Chen, Y. Li, C. Lyu, and Y. Liu, "Autonomous wi-fi relay placement with mobile robots," *IEEE/ASME Transactions on Mechatronics*, vol. 22, no. 6, pp. 2532–2542, 2017.
- [3] V. S. Varadharajan *et al.*, "Swarm Relays: Distributed Self-Healing Ground-and-Air Connectivity Chains," *IEEE Robotics and Automation Letters*, vol. 5, no. 4, pp. 5347–5354, 2020.
- [4] D. Bonilla Licea, M. Bonilla, M. Ghogho, S. Lasaulce, and V. S. Varma, "Communication-aware energy efficient trajectory planning with limited channel knowledge," *IEEE Transactions on Robotics*, vol. 36, no. 2, pp. 431–442, 2020.
- [5] U. Ali, Hong Cai, Y. Mostofi, and Y. Wardi, "Motion and communication co-optimization with path planning and online channel prediction," in *2016 American Control Conference (ACC)*, 2016, pp. 7079–7084.
- [6] A. Muralidharan and Y. Mostofi, "First passage distance to connectivity for mobile robots," in *2017 American Control Conference (ACC)*, 2017, pp. 1517–1523.
- [7] D. Bonilla Licea, M. Bonilla, M. Ghogho, and M. Malabre, "Uav trajectory planning for delay tolerant communications," in *2019 IEEE 58th Conference on Decision and Control (CDC)*, 2019, pp. 4166–4171.
- [8] U. Ali, H. Cai, Y. Mostofi, and Y. Wardi, "Motion-Communication Co-Optimization With Cooperative Load Transfer in Mobile Robotics: An Optimal Control Perspective," *IEEE Transactions on Control of Network Systems*, vol. 6, no. 2, pp. 621–632, 2019.
- [9] Y. Kantaros, M. Guo, and M. M. Zavlanos, "Temporal logic task planning and intermittent connectivity control of mobile robot networks," *IEEE Transactions on Automatic Control*, vol. 64, no. 10, pp. 4105–4120, 2019.
- [10] Y. Zeng and R. Zhang, "Energy-efficient uav communication with trajectory optimization," *IEEE Transactions on Wireless Communications*, vol. 16, no. 6, pp. 3747–3760, 2017.
- [11] Q. Wu, Y. Zeng, and R. Zhang, "Joint Trajectory and Communication Design for Multi-UAV Enabled Wireless Networks," *IEEE Transactions on Wireless Communications*, vol. 17, no. 3, pp. 2109–2121, 2018.
- [12] C. Zhan, Y. Zeng, and R. Zhang, "Energy-efficient data collection in uav enabled wireless sensor network," *IEEE Wireless Communications Letters*, vol. 7, no. 3, pp. 328–331, 2018.
- [13] X. Liu *et al.*, "Throughput Optimization of Blocked Data Transmission: A Mobile-Relay-UAV-Assisted Approach," in *IEEE International Conference on Computer and Communications*, 2019, pp. 792–796.
- [14] S. Ahmed, M. Z. Chowdhury, and Y. M. Jang, "Energy-Efficient UAV Relaying Communications to Serve Ground Nodes," *IEEE Communications Letters*, vol. 24, no. 4, pp. 849–852, 2020.
- [15] M. T. Dabiri and S. M. S. Sadough, "Optimal Placement of UAV-Assisted Free-Space Optical Communication Systems With DF Relaying," *IEEE Communications Letters*, vol. 24, no. 1, pp. 155–158, 2020.
- [16] M. I. Khalil, "Energy Efficiency Maximization of Relay Aerial Robotic Networks," *IEEE Transactions on Green Communications and Networking*, vol. 4, no. 4, pp. 1081–1090, 2020.
- [17] A. Zhou, S. Xu, S. Wang, J. Huang, S. Yang, T. Wei, X. Zhang, and H. Ma, "Robotic Millimeter-Wave Wireless Networks," *IEEE/ACM Transactions on Networking*, vol. 28, no. 4, pp. 1534–1549, 2020.
- [18] M. Debashisha and N. Enrico, "A survey on cellular-connected UAVs: Design challenges, enabling 5G/B5G innovations, and experimental advancements," *Computer Networks*, vol. 182, pp. 1–25, 2020.
- [19] Y. Zeng, Q. Wu, and R. Zhang, "Accessing from the sky: A tutorial on uav communications for 5g and beyond," *Proceedings of the IEEE*, vol. 107, no. 12, pp. 2327–2375, 2019.
- [20] S. Chung, A. A. Paranjape, P. Dames, S. Shen, and V. Kumar, "A survey on aerial swarm robotics," *IEEE Transactions on Robotics*, vol. 34, no. 4, pp. 837–855, 2018.
- [21] D. Bonilla Licea, D. McLernon, and M. Ghogho, "Mobile robot path planners with memory for mobility diversity algorithms," *IEEE Transactions on Robotics*, vol. 33, no. 2, pp. 419–431, 2017.
- [22] J. Fink, A. Ribeiro, and V. Kumar, "Robust control of mobility and communications in autonomous robot teams," *IEEE Access*, vol. 1, pp. 290–309, 2013.
- [23] M. Coppola, K. N. McGuire, C. De Wagter, and G. C. H. E. de Croon, "A survey on swarming with micro air vehicles: Fundamental challenges and constraints," *Frontiers in Robotics and AI*, vol. 7, p. 18, 2020. [Online]. Available: <https://www.frontiersin.org/article/10.3389/frobt.2020.00018>
- [24] M. Calvo-Fullana, A. Pyattaev, D. Mox, S. Andreev, and A. Ribeiro, "Communications and robotics simulation in uavs: A case study on aerial synthetic aperture antennas," *IEEE Communications Magazine*, vol. 59, no. 1, pp. 22–27, 2021.
- [25] M. Calvo-Fullana, D. Mox, A. Pyattaev, J. Fink, V. Kumar, and A. Ribeiro, "Ros-netsim: A framework for the integration of robotic and network simulators," *IEEE Robotics and Automation Letters*, vol. 6, no. 2, pp. 1120–1127, 2021.
- [26] M. Guo and M. M. Zavlanos, "Multirobot data gathering under buffer constraints and intermittent communication," *IEEE Transactions on Robotics*, vol. 34, no. 4, pp. 1082–1097, 2018.
- [27] M. Lindhe and K. H. Johansson, "Using robot mobility to exploit multipath fading," *IEEE Wireless Communications*, vol. 16, no. 1, pp. 30–37, 2009.
- [28] O. M. Bushnaq, A. Celik, H. Elsawy, M. Alouini, and T. Y. Al-Naffouri, "Aeronautical data aggregation and field estimation in iot networks: Hovering and traveling time dilemma of uavs," *IEEE Transactions on Wireless Communications*, vol. 18, no. 10, pp. 4620–4635, 2019.
- [29] Y. Sun, D. Xu, D. W. K. Ng, L. Dai, and R. Schober, "Optimal 3d-trajectory design and resource allocation for solar-powered uav communication systems," *IEEE Transactions on Communications*, vol. 67, no. 6, pp. 4281–4298, 2019.
- [30] H. Kim and B. K. Kim, "Minimum-energy trajectory planning and control on a straight line with rotation for three-wheeled omni-directional mobile robots," in *2012 IEEE/RSJ International Conference on Intelligent Robots and Systems*, 2012, pp. 3119–3124.
- [31] P. F. Mulr and C. P. Neuman, "Kinematic modeling of wheeled mobile robots," *Journal of Robotic Systems*, vol. 4, no. 2, pp. 281–340, 1987.
- [32] ———, "Kinematic modeling of wheeled mobile robots," *Journal of Robotic Systems*, vol. 8, no. 2, pp. 281–340, 1987.
- [33] B. Siciliano, L. Sciavicco, L. Villani, and G. Oriolo, *Robotics: Modelling, Planning and Control*. Springer-Verlag London Limited, 2010.
- [34] H. Kim and B. K. Kim, "Minimum-energy translational trajectory generation for differential-driven wheeled mobile robots," in *J Intell Robot Syst*, vol. 49, 2007, pp. 367–383.
- [35] A. J. Weinstein and K. L. Moore, "Pose estimation of ackerman steering vehicles for outdoors autonomous navigation," in *2010 IEEE International Conference on Industrial Technology*, 2010, pp. 579–584.
- [36] H. J. Kim and B. K. Kim, "Minimum-energy trajectory planning on a tangent for battery-powered three-wheeled omni-directional mobile robots," in *ICCAS 2010*, 2010, pp. 1701–1706.
- [37] N. Tan, Z. Zhu, and P. Yu, "Neural-network-based control of wheeled mobile manipulators with unknown kinematic models," in *2020 International Symposium on Autonomous Systems (ISAS)*, 2020, pp. 212–216.
- [38] A. P. Andrews and M. S. Grewal, *Kalman filtering: Theory and Practice Using MATLAB*. John Wiley & Sons, 2008.
- [39] U. Ali, Y. Yan, Y. Mostofi, and Y. Wardi, "An optimal control approach for communication and motion co-optimization in realistic fading environments," in *2015 American Control Conference (ACC)*, 2015, pp. 2930–2935.
- [40] H. Kim and B. K. Kim, "Minimum-energy cornering trajectory planning with self-rotation for three-wheeled omni-directional mobile robots," in *Int. J. Control Autom. Syst.*, vol. 15, 2017, p. 1857–1866.

[41] P. Tokekar, N. Karnad, and V. Isler, "Energy-optimal trajectory planning for car-like robots," *Autonomous Robots*, vol. 37, p. 279–300, 2014.

[42] S. Liu and D. Sun, "Minimizing energy consumption of wheeled mobile robots via optimal motion planning," *IEEE/ASME Transactions on Mechatronics*, vol. 19, no. 2, pp. 401–411, 2014.

[43] Yongguo Mei, Yung-Hsiang Lu, Y. C. Hu, and C. S. G. Lee, "Energy-efficient motion planning for mobile robots," in *IEEE International Conference on Robotics and Automation, 2004. Proceedings. ICRA '04. 2004*, vol. 5, 2004, pp. 4344–4349 Vol.5.

[44] —, "Deployment of mobile robots with energy and timing constraints," *IEEE Transactions on Robotics*, vol. 22, no. 3, pp. 507–522, 2006.

[45] Guiling Wang, M. J. Irwin, P. Berman, Haoying Fu, and T. La Porta, "Optimizing sensor movement planning for energy efficiency," in *ISLPED '05. Proceedings of the 2005 International Symposium on Low Power Electronics and Design, 2005.*, 2005, pp. 215–220.

[46] F. El-Moukadem, E. Torng, and G. Xing, "Mobile relay configuration in data-intensive wireless sensor networks," *IEEE Transactions on Mobile Computing*, vol. 12, no. 2, pp. 261–273, 2013.

[47] Chiping Tang and P. K. McKinley, "Energy optimization under informed mobility," *IEEE Transactions on Parallel and Distributed Systems*, vol. 17, no. 9, pp. 947–962, 2006.

[48] C. C. Ooi and C. Schindelhauer, "Minimal energy path planning for wireless robots," *Mobile Networks and Applications*, vol. 14, no. 3, pages=309-321, doi=10.1007/s11036-008-0150-5, 2009.

[49] H. Jaleel, Y. Wardi, and M. Egerstedt, "Minimizing mobility and communication energy in robotic networks: An optimal control approach," in *2014 American Control Conference*, 2014, pp. 2662–2667.

[50] Y. Mei, Y. Lu, Y. C. Hu, and C. G. Lee, "A case study of mobile robot's energy consumption and conservation techniques," in *2th International Conference on Advanced Robotics*, 2005.

[51] W. Youn and S. Andrew Gadsden, "Combined quaternion-based error state kalman filtering and smooth variable structure filtering for robust attitude estimation," *IEEE Access*, vol. 7, pp. 148 989–149 004, 2019.

[52] J. Diebel, "Representing attitude: Euler angles, unit quaternions, and rotation vectors," 2006.

[53] R. Mahony, V. Kumar, and P. Corke, "Multirotor aerial vehicles: Modeling, estimation, and control of quadrotor," *IEEE Robotics Automation Magazine*, vol. 19, no. 3, pp. 20–32, 2012.

[54] F. Morbidi, R. Cano, and D. Lara, "Minimum-energy path generation for a quadrotor uav," in *2016 IEEE International Conference on Robotics and Automation (ICRA)*, 2016, pp. 1492–1498.

[55] C. M. V. Flight Dynamics Principles. A Linear Systems Approach to Aircraft Stability and Control. Elsevier Ltd., New York, 2013.

[56] F. Yacef, N. Rizoug, L. Degaa, O. Bouhali, and M. Hamerlain, "Trajectory optimisation for a quadrotor helicopter considering energy consumption," in *2017 4th International Conference on Control, Decision and Information Technologies (CoDIT)*, 2017, pp. 1030–1035.

[57] W. Green and P. Oh, "Autonomous hovering of a fixed-wing micro air vehicle," in *Proceedings 2006 IEEE International Conference on Robotics and Automation, 2006. ICRA 2006.*, 2006, pp. 2164–2169.

[58] R. W. Beard and T. W. McLain, *Small Unmanned Aircraft: Theory and Practice*. USA: Princeton University Press, 2012.

[59] I. Lugo-Cárdenas, G. Flores, S. Salazar, and R. Lozano, "Dubins path generation for a fixed wing uav," in *2014 International Conference on Unmanned Aircraft Systems (ICUAS)*, 2014, pp. 339–346.

[60] J. W. Langelaan, N. Alley, and J. Neidhoefer, "Wind field estimation for small unmanned aerial vehicles," *Journal of Guidance, Control, and Dynamics*, vol. 34, no. 4, pp. 1016–1030, 2011. [Online]. Available: <https://doi.org/10.2514/1.52532>

[61] R. W. Beard, J. Ferrin, and J. Humphreys, "Fixed wing uav path following in wind with input constraints," *IEEE Transactions on Control Systems Technology*, vol. 22, no. 6, pp. 2103–2117, 2014.

[62] T. A. Johansen, A. Cristofaro, K. Sørensen, J. M. Hansen, and T. I. Fossen, "On estimation of wind velocity, angle-of-attack and sideslip angle of small uavs using standard sensors," in *2015 International Conference on Unmanned Aircraft Systems (ICUAS)*, 2015, pp. 510–519.

[63] K. T. Borup, B. N. Stovner, T. I. Fossen, and T. A. Johansen, "Kalman filters for air data system bias correction for a fixed-wing uav," *IEEE Transactions on Control Systems Technology*, vol. 28, no. 6, pp. 2164–2176, 2020.

[64] P. J. Nguyen-Tuong D., "Model learning for robot control: a survey," *Cognitive Process*, vol. 12, p. 319–340, 2011.

[65] A. F. Molisch, *Wireless Communications*. John Wiley & Sons Ltd, 2011.

[66] P. Liu, D. W. Matolak, B. Ai, and R. Sun, "Path loss modeling for vehicle-to-vehicle communication on a slope," *IEEE Transactions on Vehicular Technology*, vol. 63, no. 6, pp. 2954–2958, 2014.

[67] B. Sklar, "Rayleigh fading channels in mobile digital communication systems .i. characterization," *IEEE Communications Magazine*, vol. 35, no. 7, pp. 90–100, 1997.

[68] A. F. Molisch, F. Tufvesson, J. Karedal, and C. F. Mecklenbauer, "A survey on vehicle-to-vehicle propagation channels," *IEEE Wireless Communications*, vol. 16, no. 6, pp. 12–22, 2009.

[69] A. E. Forooshani, S. Bashir, D. G. Michelson, and S. Noghamian, "A survey of wireless communications and propagation modeling in underground mines," *IEEE Communications Surveys Tutorials*, vol. 15, no. 4, pp. 1524–1545, 2013.

[70] T. Rappaport, *Wireless communications: Principles and practice*, 2nd ed., ser. Prentice Hall communications engineering and emerging technologies series. Prentice Hall, 2002, includes bibliographical references and index.

[71] N. ryul Jeon, C. hoon Lee, N. gyoung Kang, and S. cheol Kim, "Performance of channel prediction using 3d ray-tracing scheme compared to conventional 2d scheme," in *Asia-Pacific Conference on Communications*, 2006.

[72] R. Zentner and A. K. Micalo, "Ray tracing interpolation for continuous modeling of double directional radio channel," in *Eurocon*, 2013.

[73] O. Stabler and R. Hoppe, "Mimo channel capacity computed with 3d ray tracing model," in *3rd European Conference on Antennas and Propagation*, 2009.

[74] S. Y. Seidel and T. S. Rappaport, "914 mhz path loss prediction models for indoor wireless communications in multifloored buildings," *IEEE Transactions on Antennas and Propagation*, vol. 40, no. 2, pp. 207–217, 1992.

[75] Kwok-Wai Cheung, J. H. . Sau, and R. D. Murch, "A new empirical model for indoor propagation prediction," *IEEE Transactions on Vehicular Technology*, vol. 47, no. 3, pp. 996–1001, 1998.

[76] Y. Mostofi, M. Malmirchegini, and A. Ghaffarkhah, "Estimation of communication signal strength in robotic networks," in *2010 IEEE International Conference on Robotics and Automation*, 2010, pp. 1946–1951.

[77] M. Malmirchegini and Y. Mostofi, "On the spatial predictability of communication channels," *IEEE Transactions on Wireless Communications*, vol. 11, no. 3, pp. 964–978, 2012.

[78] M. Gudmundson, "Correlation model for shadow fading in mobile radio systems," *Electronics Letters*, vol. 27, pp. 2145–2146(1), November 1991.

[79] F. Baccelli and X. Zhang, "A correlated shadowing model for urban wireless networks," in *2015 IEEE Conference on Computer Communications (INFOCOM)*, 2015, pp. 801–809.

[80] R. D. A. Timoteo, D. C. Cunha, and G. D. C. Cavalcanti, "A proposal for path loss prediction in urban environments using support vector regression," in *ICT 2014*, 2014.

[81] N. C. Beaulieu and M. Naseri, "A circuit theory model for shadow fading autocorrelation in wireless radio channels," *IEEE Wireless Communications Letters*, vol. 8, no. 1, pp. 161–164, 2019.

[82] Xiaodong Cai and G. B. Giannakis, "A two-dimensional channel simulation model for shadowing processes," *IEEE Transactions on Vehicular Technology*, vol. 52, no. 6, pp. 1558–1567, 2003.

[83] M. K. Simon and M.-S. Alouini, *Digital Communication over Fading Channels*. John Wiley & Sons Ltd, 2005.

[84] A. Ghaffarkhah and Y. Mostofi, "Communication-aware motion planning in mobile networks," *IEEE Transactions on Automatic Control*, vol. 56, no. 10, pp. 2478–2485, 2011.

[85] W. C. Jakes, *Microwave Mobile Communications*. IEEE Press, 1974.

[86] Yahong Rosa Zheng and Chengshan Xiao, "Simulation models with correct statistical properties for rayleigh fading channels," *IEEE Transactions on Communications*, vol. 51, no. 6, pp. 920–928, 2003.

[87] A. J. Carfang, N. Wagle, and E. W. Frew, "Improving data ferrying by iteratively learning the radio frequency environment," in *2014 IEEE/RSJ International Conference on Intelligent Robots and Systems*, 2014, pp. 1182–1188.

[88] S. K. Goudos and G. Athanasiadou, "Application of an ensemble method to uav power modeling for cellular communications," *IEEE Antennas and Wireless Propagation Letters*, vol. 18, no. 11, pp. 2340–2344, 2019.

[89] J. Chen, U. Yatnalli, and D. Gesbert, "Learning radio maps for uav-aided wireless networks: A segmented regression approach," in *2017 IEEE International Conference on Communications (ICC)*, 2017, pp. 1–6.

[90] Y. Egi and C. E. Otero, "Machine-learning and 3d point-cloud based signal power path loss model for the deployment of wireless communication systems," *IEEE Access*, vol. 7, pp. 42 507–42 517, 2019.

[91] E. Ostlin, H. Zepernick, and H. Suzuki, "Macrocell path-loss prediction using artificial neural networks," *IEEE Transactions on Vehicular Technology*, vol. 59, no. 6, pp. 2735–2747, 2010.

[92] P. S. Bithas, E. T. Michailidis, N. Nomikos, D. Vouyioukas, and A. G. Kanatas, "A survey on machine-learning techniques for uav-based communications," *Sensors*, vol. 19, no. 23, 2019. [Online]. Available: <https://www.mdpi.com/1424-8220/19/23/5170>

[93] A. A. Khuwaja, Y. Chen, N. Zhao, M. Alouini, and P. Dobbins, "A survey of channel modeling for uav communications," *IEEE Communications Surveys Tutorials*, vol. 20, no. 4, pp. 2804–2821, 2018.

[94] W. Khawaja, I. Guvenc, D. W. Matolak, U. C. Fiebig, and N. Schneckenburger, "A survey of air-to-ground propagation channel modeling for unmanned aerial vehicles," *IEEE Communications Surveys Tutorials*, vol. 21, no. 3, pp. 2361–2391, 2019.

[95] M. Asadpour, B. Van den Bergh, D. Giustiniano, K. A. Hummel, S. Pollin, and B. Plattner, "Micro aerial vehicle networks: an experimental analysis of challenges and opportunities," *IEEE Communications Magazine*, vol. 52, no. 7, pp. 141–149, 2014.

[96] E. Yanmaz, R. Kuschnig, and C. Bettstetter, "Channel measurements over 802.11a-based uav-to-ground links," in *2011 IEEE GLOBECOM Workshops (GC Wkshps)*, 2011, pp. 1280–1284.

[97] N. Ahmed, S. S. Kanhere, and S. Jha, "On the importance of link characterization for aerial wireless sensor networks," *IEEE Communications Magazine*, vol. 54, no. 5, pp. 52–57, 2016.

[98] C. Cheng, P. Hsiao, H. T. Kung, and D. Vlah, "Performance measurement of 802.11a wireless links from uav to ground nodes with various antenna orientations," in *Proceedings of 15th International Conference on Computer Communications and Networks*, 2006, pp. 303–308.

[99] E. Yanmaz, R. Kuschnig, and C. Bettstetter, "Achieving air-ground communications in 802.11 networks with three-dimensional aerial mobility," in *2013 Proceedings IEEE INFOCOM*, 2013, pp. 120–124.

[100] J. Chen, D. Raye, W. Khawaja, P. Sinha, and I. Guvenc, "Impact of 3d uwb antenna radiation pattern on air-to-ground drone connectivity," in *2018 IEEE 88th Vehicular Technology Conference (VTC-Fall)*, 2018, pp. 1–5.

[101] Q. Zhang, M. Mozaffari, W. Saad, M. Bennis, and M. Debbah, "Machine learning for predictive on-demand deployment of uavs for wireless communications," in *2018 IEEE Global Communications Conference (GLOBECOM)*, 2018, pp. 1–6.

[102] H. E. Hammouti and M. Ghogho, "Air-to-ground channel modeling for uav communications using 3d building footprints," in *Ubiquitous Networking*, N. Boudriga, M.-S. Alouini, S. Rekhis, E. Sabir, and S. Pollin, Eds. Cham: Springer International Publishing, 2018, pp. 372–383.

[103] N. Goddemeier and C. Wietfeld, "Investigation of air-to-air channel characteristics and a uav specific extension to the rice model," in *2015 IEEE Globecom Workshops (GC Wkshps)*, 2015, pp. 1–5.

[104] A. Zanella, "Best practice in rss measurements and ranging," *IEEE Communications Surveys Tutorials*, vol. 18, no. 4, pp. 2662–2686, 2016.

[105] M. Lindhe and K. H. Johansson, "Communication-aware trajectory tracking," in *2008 IEEE International Conference on Robotics and Automation*, 2008, pp. 1519–1524.

[106] C. E. Shannon, "A mathematical theory of communication," *The Bell System Technical Journal*, vol. 27, no. 3, pp. 379–423, 1948.

[107] A. Goldsmith, *Wireless Communications*. Stanford University, 2004.

[108] S. Yarkan, S. Guzelgoz, H. Arslan, and R. R. Murphy, "Underground mine communications: A survey," *IEEE Communications Surveys Tutorials*, vol. 11, no. 3, pp. 125–142, 2009.

[109] A. Hrovat, G. Kandus, and T. Javornik, "A survey of radio propagation modeling for tunnels," *IEEE Communications Surveys Tutorials*, vol. 16, no. 2, pp. 658–669, 2014.

[110] M. M. Azari, G. Geraci, A. Garcia-Rodriguez, and S. Pollin, "Cellular uav-to-uav communications," in *2019 IEEE 30th Annual International Symposium on Personal, Indoor and Mobile Radio Communications (PIMRC)*, 2019, pp. 1–7.

[111] S. Boyd and L. Vandenberghe, *Convex Optimization*. Cambridge University Press, 2004.

[112] E. Rossi, M. Bruschetta, R. Carli, Y. Chen, and M. Farina, "Online nonlinear model predictive control for tethered uavs to perform a safe and constrained maneuver," in *2019 18th European Control Conference (ECC)*, 2019, pp. 3996–4001.

[113] Y. Yan and Y. Mostofi, "To go or not to go: On energy-aware and communication-aware robotic operation," *IEEE Transactions on Control of Network Systems*, vol. 1, no. 3, pp. 218–231, 2014.

[114] D. B. Licea, D. McLernon, M. Ghogho, and S. A. R. Zaidi, "An energy saving robot mobility diversity algorithm for wireless communications," in *21st European Signal Processing Conference (EUSIPCO 2013)*, 2013, pp. 1–5.

[115] D. Bonilla Licea, D. McLernon, and M. Ghogho, "Designing optimal trajectory planners for robotic communications," in *IET Intelligent Signal Processing Conference 2013 (ISP 2013)*, 2013, pp. 1–6.

[116] A. Muralidharan and Y. Mostofi, "Path planning for a connectivity seeking robot," in *2017 IEEE Globecom Workshops (GC Wkshps)*, 2017, pp. 1–6.

[117] —, "Distributed beamforming using mobile robots," in *2016 IEEE International Conference on Acoustics, Speech and Signal Processing (ICASSP)*, 2016, pp. 6385–6389.

[118] A. Mardani, M. Chiaberge, and P. Giaccone, "Communication-aware uav path planning," *IEEE Access*, vol. 7, pp. 52 609–52 621, 2019.

[119] S. De Bast, E. Vinogradov, and S. Pollin, "Cellular coverage-aware path planning for uavs," in *2019 IEEE 20th International Workshop on Signal Processing Advances in Wireless Communications (SPAWC)*, 2019, pp. 1–5.

[120] D. B. Licea, V. S. Varma, S. Lasaulce, J. Daafouz, and M. Ghogho, "Trajectory planning for energy-efficient vehicles with communications constraints," in *2016 International Conference on Wireless Networks and Mobile Communications (WINCOM)*, 2016, pp. 264–270.

[121] D. B. Licea, V. S. Varma, S. Lasaulce, J. Daafouz, M. Ghogho, and D. McLernon, "Robust trajectory planning for robotic communications under fading channels," in *Ubiquitous Networking*, E. Sabir, A. García Armada, M. Ghogho, and M. Debbah, Eds. Cham: Springer International Publishing, 2017, pp. 450–460.

[122] A. Muralidharan and Y. Mostofi, "Communication-aware robotics: Exploiting motion for communication," *Annual Review of Control, Robotics, and Autonomous Systems*, vol. 4, no. 1, pp. 115–139, 2021. [Online]. Available: <https://doi.org/10.1146/annurev-control-071420-080708>

[123] E. Stump, A. Jadabaaie, and V. Kumar, "Connectivity management in mobile robot teams," in *2008 IEEE International Conference on Robotics and Automation*, 2008, pp. 1525–1530.

[124] O. Tekdas and V. Isler, "Robotic routers," in *2008 IEEE International Conference on Robotics and Automation*, 2008, pp. 1513–1518.

[125] H. Oh, H. Shin, S. Kim, P. Ladosz, and W. Chen, "Communication-aware convoy following guidance for uavs in a complex urban environment," in *2016 24th Mediterranean Conference on Control and Automation (MED)*, 2016, pp. 1230–1235.

[126] Y. Zeng, R. Zhang, and T. J. Lim, "Throughput maximization for uav-enabled mobile relaying systems," *IEEE Transactions on Communications*, vol. 64, no. 12, pp. 4983–4996, 2016.

[127] K. Kim, K. G. Shin, and D. Niculescu, "Mobile autonomous router system for dynamic (re)formation of wireless relay networks," *IEEE Transactions on Mobile Computing*, vol. 12, no. 9, pp. 1828–1841, 2013.

[128] D. Bonilla Licea, E. Nurellari, and M. Ghogho, "Energy balancing for robotic aided clustered wireless sensor networks using mobility diversity algorithms," in *2018 26th European Signal Processing Conference (EUSIPCO)*, 2018, pp. 1815–1819.

[129] E. Nurellari, D. B. Licea, and M. Ghogho, "Optimum trajectory planning for robotic data ferries in delay tolerant wireless sensor networks," in *2019 27th European Signal Processing Conference (EUSIPCO)*, 2019, pp. 1–5.

[130] D. Bonilla Licea, E. Nurellari, and M. Ghogho, "Energy-efficient 3d uav trajectory design for data collection in wireless sensor networks," in *ICASSP 2020 - 2020 IEEE International Conference on Acoustics, Speech and Signal Processing (ICASSP)*, 2020, pp. 8329–8333.

[131] Y. Sun, D. Xu, D. W. K. Ng, L. Dai, and R. Schober, "Optimal 3d trajectory design and resource allocation for solar-powered uav communication systems," *IEEE Transactions on Communications*, vol. 67, no. 6, pp. 4281–4298, 2019.

[132] L. Chiaraviglio, F. D'andreagiovanni, R. Choo, F. Cuomo, and S. Colonnese, "Joint optimization of area throughput and grid-connected microgeneration in uav-based mobile networks," *IEEE Access*, vol. 7, pp. 69 545–69 558, 2019.

[133] A. Alsharoa, H. Ghazzai, A. Kadri, and A. E. Kamal, "Spatial and temporal management of cellular hetnets with multiple solar powered drones," *IEEE Transactions on Mobile Computing*, vol. 19, no. 4, pp. 954–968, 2020.

- [134] W. Burgard, O. Brock, and C. Stachniss, *An Experimental Study of Exploiting Multipath Fading for Robot Communications*, 2008, pp. 289–296.
- [135] D. Puccinelli and M. Haenggi, “Spatial diversity benefits by means of induced fading,” in *2006 3rd Annual IEEE Communications Society on Sensor and Ad Hoc Communications and Networks*, vol. 1, 2006, pp. 128–137.
- [136] D. Bonilla Licea, S. A. Raza Zaidi, D. McLernon, and M. Ghogho, “Improving radio energy harvesting in robots using mobility diversity,” *IEEE Transactions on Signal Processing*, vol. 64, no. 8, pp. 2065–2077, 2016.
- [137] D. B. Licea, D. McLernon, M. Ghogho, E. Nurellari, and S. A. Raza Zaidi, “Robotic mobility diversity algorithm with continuous search space,” in *2018 26th European Signal Processing Conference (EUSIPCO)*, 2018, pp. 702–706.
- [138] D. Bonilla Licea, M. Ghogho, D. McLernon, and S. A. R. Zaidi, “Mobility diversity-assisted wireless communication for mobile robots,” *IEEE Transactions on Robotics*, vol. 32, no. 1, pp. 214–229, 2016.
- [139] D. B. Licea, M. Ghogho, D. McLernon, and S. A. R. Zaidi, “Antenna controller for low-latency and high reliability robotic communications over time-varying fading channels,” in *2019 27th European Signal Processing Conference (EUSIPCO)*, 2019, pp. 1–5.
- [140] G. Geraci, A. Garcia-Rodriguez, L. G. Giordano, D. Lopez-Perez, and E. Bjoernson, “Supporting uav cellular communications through massive mimo,” in *2018 IEEE International Conference on Communications Workshops (ICC Workshops)*, 2018, pp. 1–6.
- [141] A. Farajzadeh, O. Ercetin, and H. Yanikomeroglu, “Uav data collection over noma backscatter networks: Uav altitude and trajectory optimization,” in *ICC 2019 - 2019 IEEE International Conference on Communications (ICC)*, 2019, pp. 1–7.
- [142] Y. Chen, N. Li, C. Wang, W. Xie, and J. Xv, “A 3d placement of unmanned aerial vehicle base station based on multi-population genetic algorithm for maximizing users with different qos requirements,” in *2018 IEEE 18th International Conference on Communication Technology (ICCT)*, 2018, pp. 967–972.
- [143] R. I. Bor-Yaliniz, A. El-Keyi, and H. Yanikomeroglu, “Efficient 3-d placement of an aerial base station in next generation cellular networks,” in *2016 IEEE International Conference on Communications (ICC)*, 2016, pp. 1–5.
- [144] H. Shakhatreh, A. Khreishah, A. Alsarhan, I. Khalil, A. Sawalmeh, and N. S. Othman, “Efficient 3d placement of a uav using particle swarm optimization,” in *2017 8th International Conference on Information and Communication Systems (ICICS)*, 2017, pp. 258–263.
- [145] H. El Hammouti, M. Benjillali, B. Shihada, and M. Alouini, “Learn-as-you-fly: A distributed algorithm for joint 3d placement and user association in multi-uavs networks,” *IEEE Transactions on Wireless Communications*, vol. 18, no. 12, pp. 5831–5844, 2019.
- [146] L. J. Rodriguez, N. H. Tran, T. Q. Duong, T. Le-Ngoc, M. Elkashlan, and S. Shetty, “Physical layer security in wireless cooperative relay networks: state of the art and beyond,” *IEEE Communications Magazine*, vol. 53, no. 12, pp. 32–39, 2015.
- [147] X. Sun, D. W. K. Ng, Z. Ding, Y. Xu, and Z. Zhong, “Physical layer security in uav systems: Challenges and opportunities,” *IEEE Wireless Communications*, vol. 26, no. 5, pp. 40–47, 2019.
- [148] X. Sun, C. Shen, T.-H. Chang, and Z. Zhong, “Joint resource allocation and trajectory design for uav-aided wireless physical layer security,” in *2018 IEEE Globecom Workshops (GC Wkshps)*, 2018, pp. 1–6.
- [149] X. Sun, C. Shen, D. W. K. Ng, and Z. Zhong, “Robust trajectory and resource allocation design for secure uav-aided communications,” in *2019 IEEE International Conference on Communications Workshops (ICC Workshops)*, 2019, pp. 1–6.
- [150] A. Li, Q. Wu, and R. Zhang, “Uav-enabled cooperative jamming for improving secrecy of ground wiretap channel,” *IEEE Wireless Communications Letters*, vol. 8, no. 1, pp. 181–184, 2019.
- [151] Y. Cai, F. Cui, Q. Shi, M. Zhao, and G. Y. Li, “Dual-uav-enabled secure communications: Joint trajectory design and user scheduling,” *IEEE Journal on Selected Areas in Communications*, vol. 36, no. 9, pp. 1972–1985, 2018.
- [152] Y. Zhou, P. L. Yeoh, H. Chen, Y. Li, R. Schober, L. Zhuo, and B. Vucetic, “Improving physical layer security via a uav friendly jammer for unknown eavesdropper location,” *IEEE Transactions on Vehicular Technology*, vol. 67, no. 11, pp. 11 280–11 284, 2018.
- [153] C. Liu, J. Lee, and T. Q. S. Quek, “Safeguarding uav communications against full-duplex active eavesdropper,” *IEEE Transactions on Wireless Communications*, vol. 18, no. 6, pp. 2919–2931, 2019.